Compendium

ThermoFisher SCIENTIFIC

Analytical techniques in polymer analysis:

FTIR and Raman spectroscopy and microscopy

thermo scientific

Introduction

In the development of new polymer materials with novel properties, quick and trustworthy analysis is essential. FTIR and Raman spectroscopy and microscopy can address this need: FTIR spectroscopy is able to identify chemical structures and functional groups within polymers, providing detailed information about the molecular composition and chemical bonds by measuring the absorption of infrared light at various wavelengths. Raman microscopy, on the other hand, complements FTIR by using inelastic scattering of monochromatic light (from a laser source) to obtain vibrational, rotational, and other low-frequency modes. For polymer samples, these techniques can help to characterize crystalline structures, analyze the distribution of different polymer components, determine density or the level of curing, and more.

This compendium highlights multiple ways in which these powerful analytical techniques contribute to practical understanding and real-world solutions for a range of issues. In the section on microscopy, articles describe how FTIR microscopy can be applied to PET and HDPE to characterize contaminants during the recycling process, and how infrared microscopy can perform chemical characterization of artificial fibers. These are just a couple examples of how these analytical techniques help to improve the quality of polymer-based materials while reducing pollution in the environment.

The different and complementary benefits of Raman and FTIR microscopy mapping and imaging are explored in articles about the investigation of layered polymer composites, while combined Raman and FTIR spectroscopy techniques are used to analyze laminate materials. Raman microscopy can even perform in situ determination of polymer density, as is shown in an article about polyethylene in multi-layer polymer films.

FTIR and FT-NIR spectroscopy can provide essential polymer production information, especially around aspects like UV curing or polymerization cure rates. These techniques provide feedback at a rate rapid enough to allow time-based monitoring of the curing process, which could have a sizable impact on production efficiency.

Together or separately, the non-invasive, non-destructive analytical techniques of FTIR and Raman spectroscopy and microscopy offer comprehensive insights into the chemical and structural properties of polymers. This crucial information aids in quality control, material development, and failure analysis. The articles and research papers in this compendium provide detailed examples about the effectiveness of these advanced analytical techniques and their utility for the polymer industry.

Table of contents

Microscopy

Complementary use of Raman and FTIR imaging for multi-layer polymer composite analysis

Authors
Robert Heintz, Mark Wall, Jennifer Ramirez, Stephan Woods

Thermo Fisher Scientific, Madison, WI

Overview

Purpose: To compare and contrast the benefits of FTIR and Raman microscopy mapping and imaging for the analysis of layered polymer composites.

Methods: FTIR and dispersive Raman microscopes were used to analyze multi-layered polymer composite materials.

Results: An important advantage of FTIR microspectroscopy is that the spectra highlight polar functional groups which are particularly important when characterizing different types of polymers. A large number of FTIR spectral data bases are available for identification of polymeric materials.

Raman micro-spectroscopy offers excellent spatial resolution as well as convenient sampling options. Raman spectroscopy tends to highlight molecular backbone structure and is sensitive to molecular structure. Raman spectroscopy typically provides access to a greater spectral range that is useful for analyzing a wider range of different types of materials such as pigments.

These techniques work very well together and provide complementary information, so rather than considering these as an either or proposition, a concerted approach using both FTIR and Raman imaging would be an excellent solution for the analysis of layered polymer composites.

Introduction

A variety of different industries utilize multi-layered polymer composites specifically engineered for particular performance characteristics. Confirming the composition and integrity of these materials is important both for the industries that manufacture these products as well as for industries that utilize these materials in their own products. The diversity of the materials used and the microscopic construction of these materials requires analytical techniques with unique capabilities.

Raman and FTIR micro-spectroscopy are both uniquely suited for the analysis of polymer composites. They both can be used to readily identify unknown materials as well as providing information on molecular structure and chemical environment. Microscopic applications are available for both of these techniques even though there are some difference in the expected spatial resolutions. FTIR and Raman mapping and imaging provide a convenient way to visualize the distribution of components or differences in molecular structure in polymer composites. Each of these analytical methods has its own advantages and challenges associated with it. Raman and FTIR spectroscopy should not be viewed as mutually exclusive; rather than choosing between the two, a better approach would be to view them as complementary and to use both to get a much better overall understanding of the samples.

Methods

Vibrational spectroscopy

A Thermo Scientific™ DXRxi Raman imaging microscope was used to collect the Raman imaging data. The transmission FTIR mapping data was obtained using a Thermo Scientific™ Nicolet™ iN10 FTIR microscope. The attenuated total reflectance (ATR) imaging data was obtained using a Thermo Scientific™ Nicolet™ iN10 MX FTIR microscope and imaging ATR accessory for microscopy.

Sample preparation

The cross-sectioned samples for Raman analysis were prepared using the Thermo Scientific™ Polymer Slicing Tool for DXR Raman microscopes. For confocal depth profiling experiments the polymer films were mounted flat across a small hole in a microscope slide. For FTIR transmission analysis the samples were cross-sectioned by hand using razor blades and mounted in a Thermo Scientific micro-compression cell with diamond windows. Cross-sectioned slices of the layered composites were used for the ATR analyses.

Results

Figure 1 shows the results of a FTIR transmission mapping analysis of a layered polymer film. Five distinct layers were identified with two of the layers being the same material (polyamide). While it was relatively easy to identify the layers from the FTIR spectra, it is clear that the sample preparation has resulted in layer deformation. It may be possible to prepare these types of samples using a microtome to get the samples thin enough for transmission analysis samples thinner without having to use as much as compression but that type of sample preparation requires more extensive experience and specialized equipment. The FTIR spectra show diagnostic peaks for functional groups such as the amide peaks and the hydroxyl peak. The chemical images of the layers were generated based on correlation profiles.

One advantage of FTIR analysis is the different modes of data collection available. ATR has the advantage of requiring less sample preparation and the potential to achieve higher spatial resolution due to the higher index of refraction of the ATR crystal. An example of ATR imaging is shown in Figure 2. These results show that even the very thin polyurethane adhesive layers could be distinguished. These layers were expected to be three µm thick instead of five. This is probably due to sample deformation by ATR crystal.

Video Image of the cross- section; FTIR image superimposed showing Nylon 6 layers.

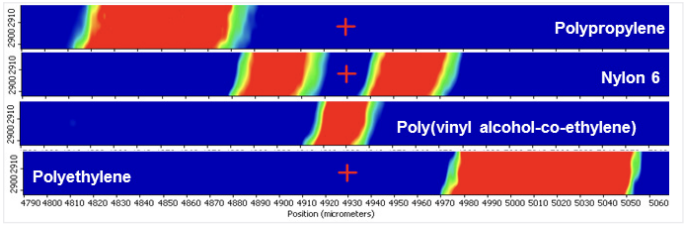

FTIR profile images showing components distributions.

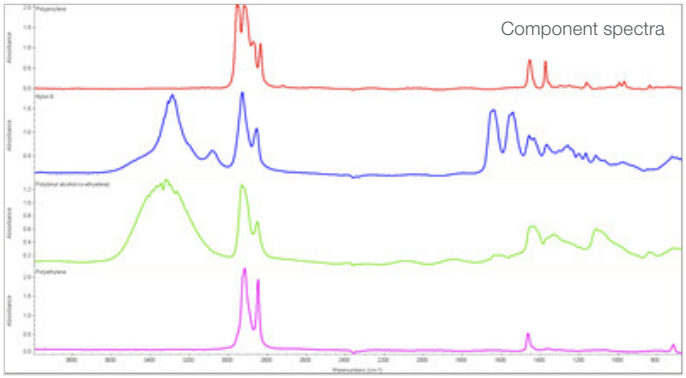

Figure 1. FTIR transmission analysis. Mapping parameters: Nicolet iN10 – transmission mode; Cross-sectioned sample; Mounted on a diamond window; Area: 280 x 20 µm; Aperture: 5 x 20 µm; Step Size: X: 2.0 µm, Y: 5.0µm; 750 spectra.

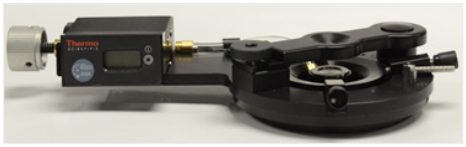

Imaging ATR accessory for microscopy.

Video image before contact.

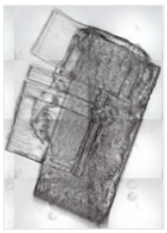

Sample deformation & delamination

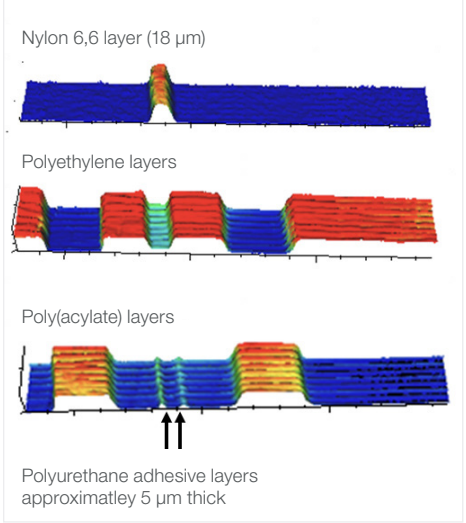

Figure 2. ATR imaging of a layered polymer composite. Imaging parameters: Nicolet iN10 MX with linear array detector; imaging ATR accessory for microscopy; effective area 412 x 43 µm; 7685 spectra.

Figure 3 show the results of Raman imaging a new portion of the film that was used in Figure 1. The Raman imaging analysis required much less sample preparation (sample thickness is not an issue) and the spatial resolution is significantly better.

There was no evidence of sample deformation and analysis does not require any sample contact. However, the Raman spectra do not have the strong peaks for the polar functionalities that are present in the FTIR spectra, making identification of the polymer materials more challenging in some cases (for instance with the poly(ethylene vinyl alcohol) layer). It is also possible to do confocal depth analysis of polymers using Raman imaging without the need to cross-section the sample (see Figure 4). However, while this is more expedient the results are often better using cross-sections.

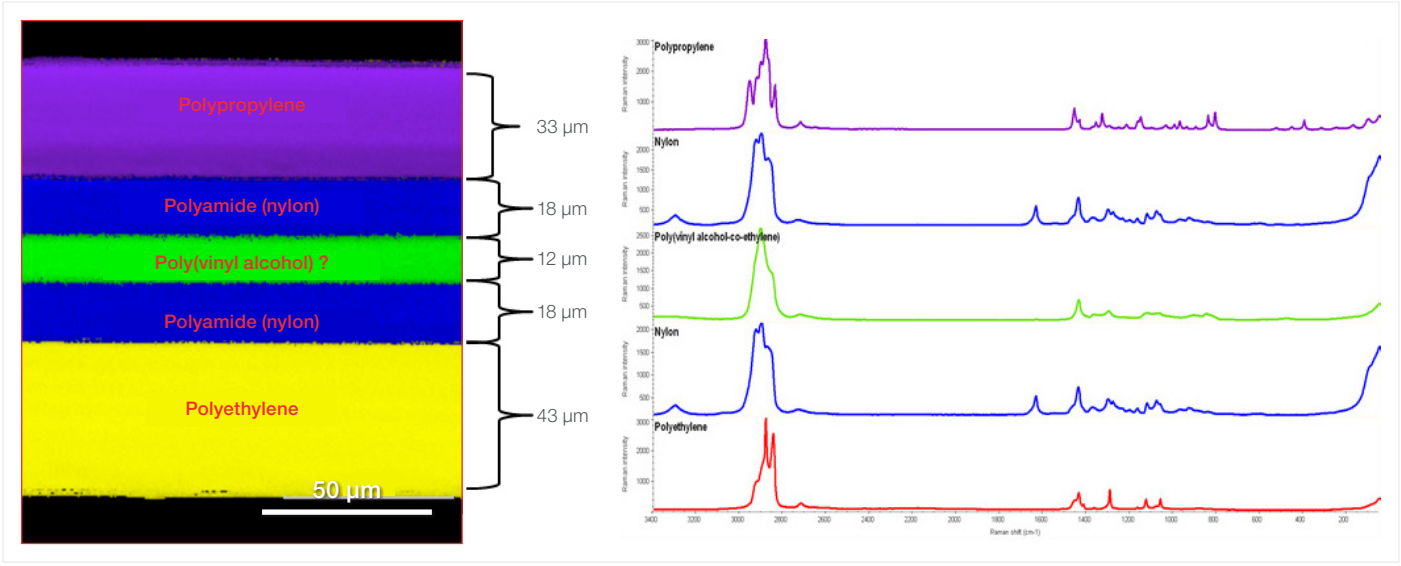

Figure 3. Raman imaging of a layered polymer film. Collection parameters: DXRxi Raman imaging microscope, 532 nm laser (10 mW), 132 x 150 µm area, 0.5 µm image pixel size, 79200 spectra, 0.020 s exposure time, 3 scans.

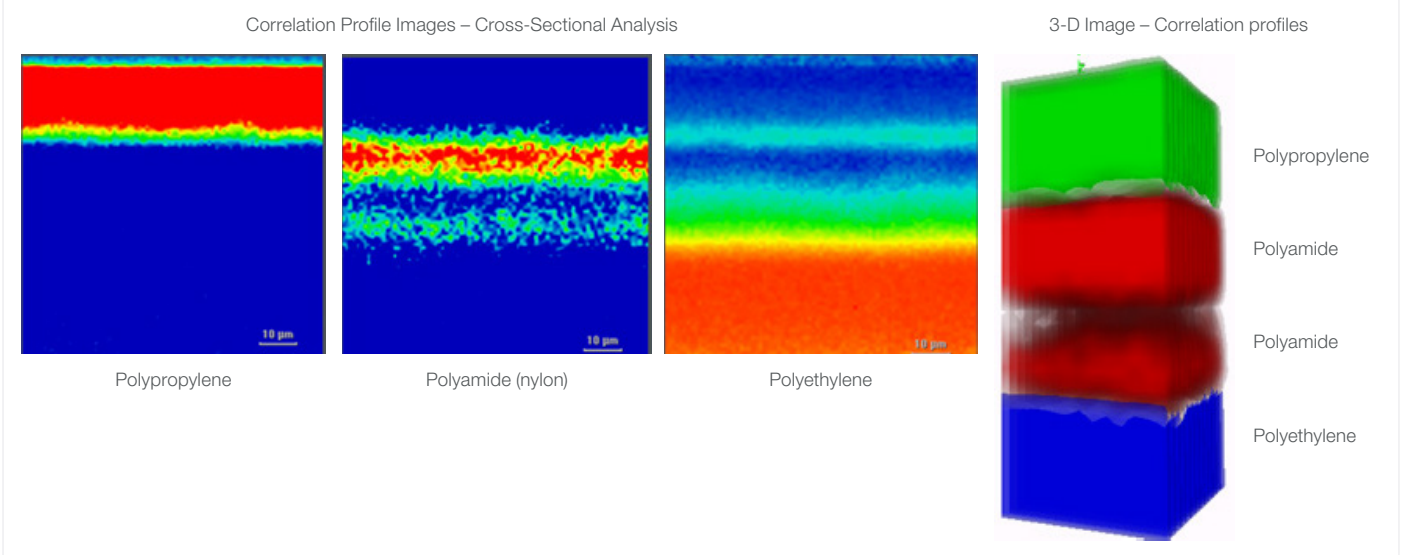

Figure 4. Confocal depth imaging of a layered polymer composite.

Combining both FTIR mapping & Raman imaging

The complementary nature of these two forms of vibrational spectroscopy can be illustrated from the analysis of the blue polymer film shown in Figures 5 and 6. The FTIR transmission analysis involved crosssectioning the sample by hand and compressing the cross-section between two diamond windows. This was done to flatten the sample and to slightly compress the film to make the whole cross-section thinner. The sample area shown in Figure 5 was mapped using transmission analysis with an aperture that was 5 x 20 µm and using step sizes of 2 µm in the X direction and 5 µm in the Y direction. The image was formed from 576 individual spectra. The chemical images shown are the result of either correlation or peak height profiles.

Four distinct layers were identified using these profiles. The first was a layer of predominately polyethylene with a smaller amount of vinyl acetate co-polymerized. The second layer, very similar to the first, but displayed a clear hydroxyl peak indicating an additional component in this layer that is consistent with co-polymerized vinyl alcohol. The third layer was a polyamide (polyamide 11). The spectra from the final layer were consistent with a co-polymer of ethylene, butyl arcylate and maleic anhydride. The borders between the layers are not distinct. It is not clear if this is a result of the sample preparation (deformation) or spatial resolution limitations.

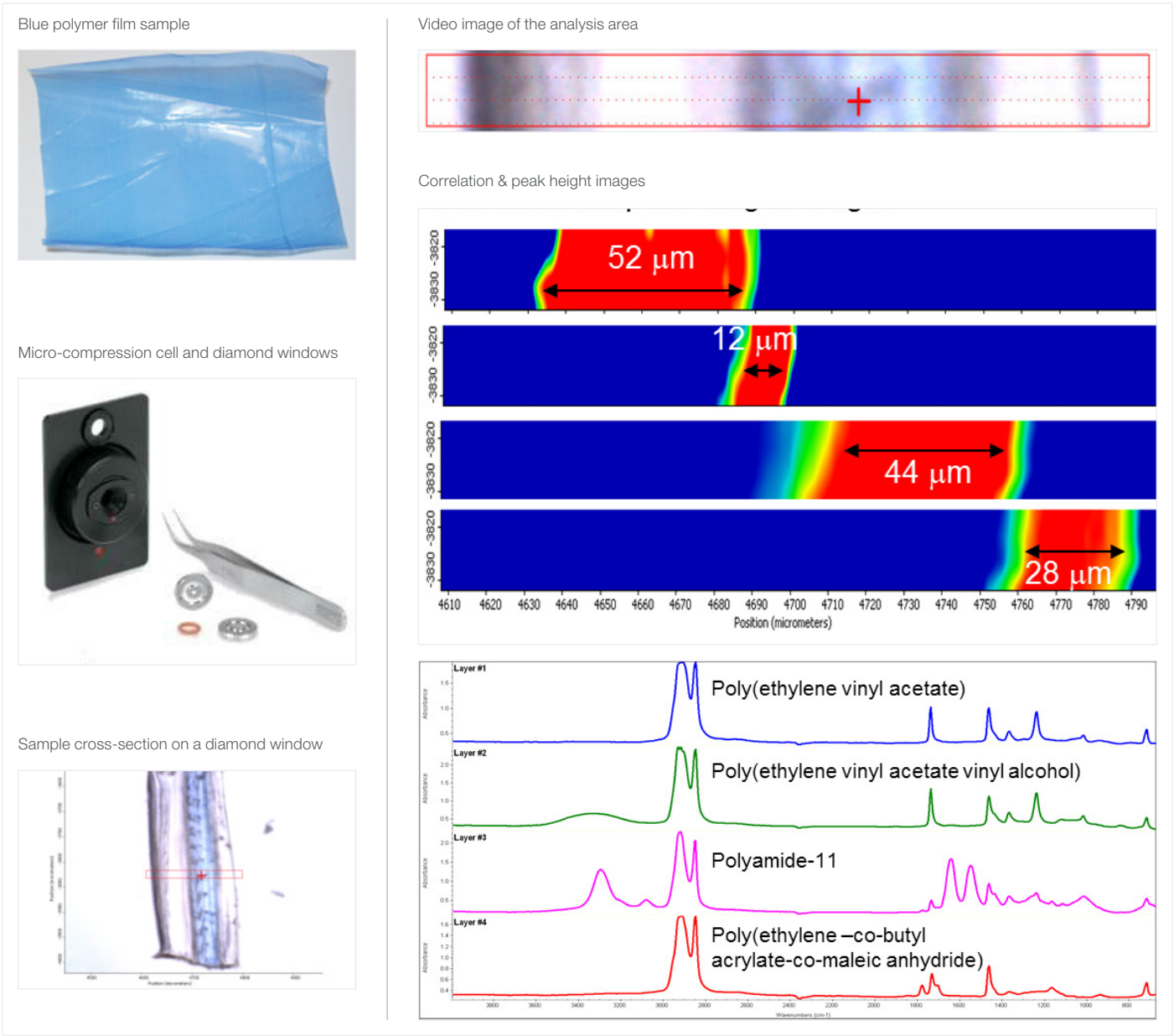

Figure 5. FTIR Mapping of a blue polymer composite film.

Raman imaging results on the same sample are shown in Figure 6. The sample was prepared using the polymer slicing tool shown. This tool allows for a flat, even crosssection of the film and also serves as the sample holder during the analysis. A visual image of the side view of the film is shown in the figure. The area imaged was 88 x 20 µm and the image pixel size was 0.5 µm. The image is made up of 7262 spectra.

Lower laser power (0.5 mW) was used because the lazurite pigment is very susceptible to laser damage. The exposure time was 0.1 s and 100 scans were averaged. Figure 6 shows five distinct layers. The chemical images are the result of either correlation or multivariate curve resolution (MCR) profiles. The MCR profile did not identify some of the layers as different components because the spectral differences were very minor. Layer #1 looks like polyethylene but has a very small peak at 1738 cm-1 (Figure 7), consistent with co-polymerized vinyl acetate. Layer #2 appears very much like polyamide but does not show the amide peaks; it does not show any hydroxyl peaks but seems to be consistent with poly(vinyl alcohol).

Based on FTIR spectra, this is likely what it is. Layer #3 looks very much like polyethylene but there is a small peak consistent with traces of lazurite. The lazurite is predominately found in layer #4. It appears to be mixed with a polyamide (Figure 8). The lazurite was unexpected and not observed in the FTIR analysis but is consistent with the blue color of the polymer film. The majority of the lazurite appears to be homogenously dispersed throughout layer 4. However, there were some larger (< 3 µm) lazurite particles observed (Figure 8). The final layer appears to be polyethylene from the Raman spectra and there is no evidence for the butyl acrylate or the maleic anhydride observed in the FTIR spectra. While Raman imaging provides greater resolution, better definition of the layers, and no layer deformation due to sample preparation, and gives evidence to the nature of the blue pigment, it does not do as well with identifying the polar functional groups of some of the co-polymerized components. These might be inferred from the Raman spectra but are confirmed by the FTIR spectra.

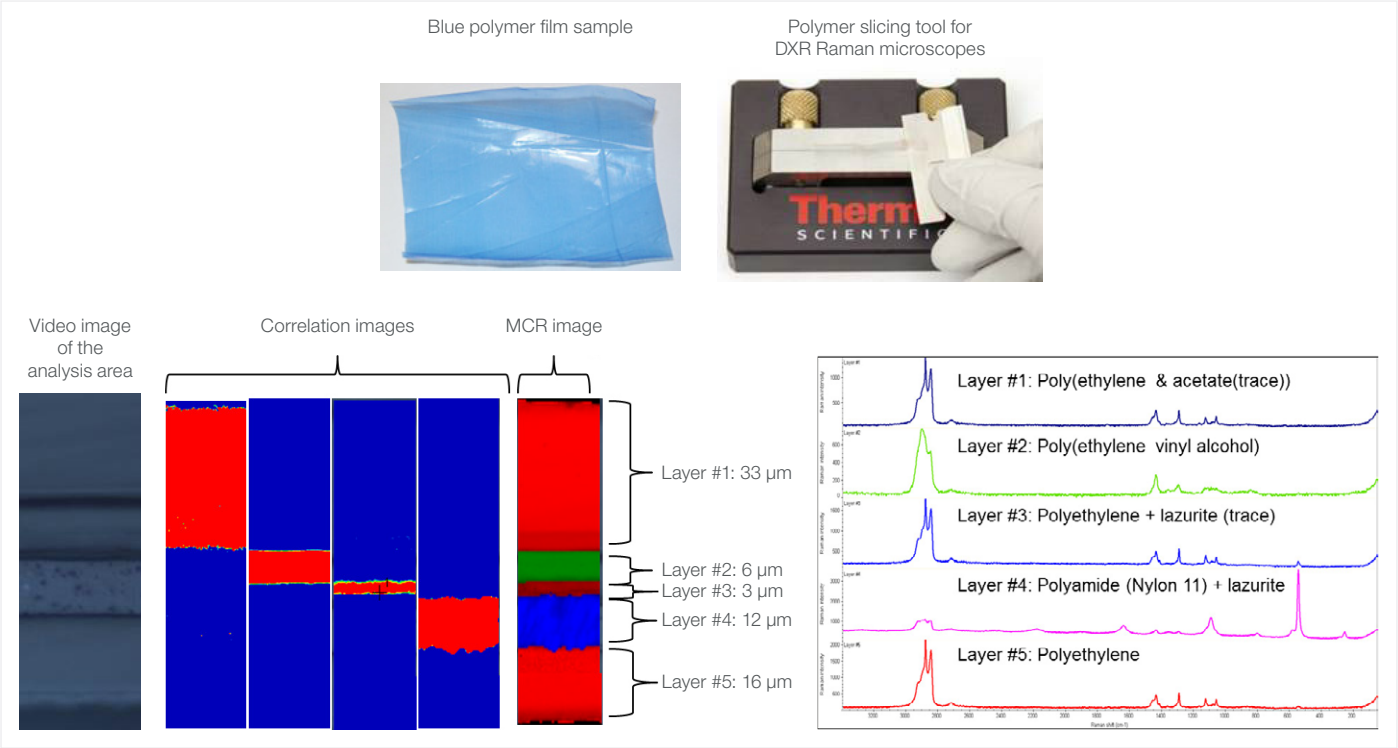

Figure 6. Raman imaging of a blue polymer composite film.

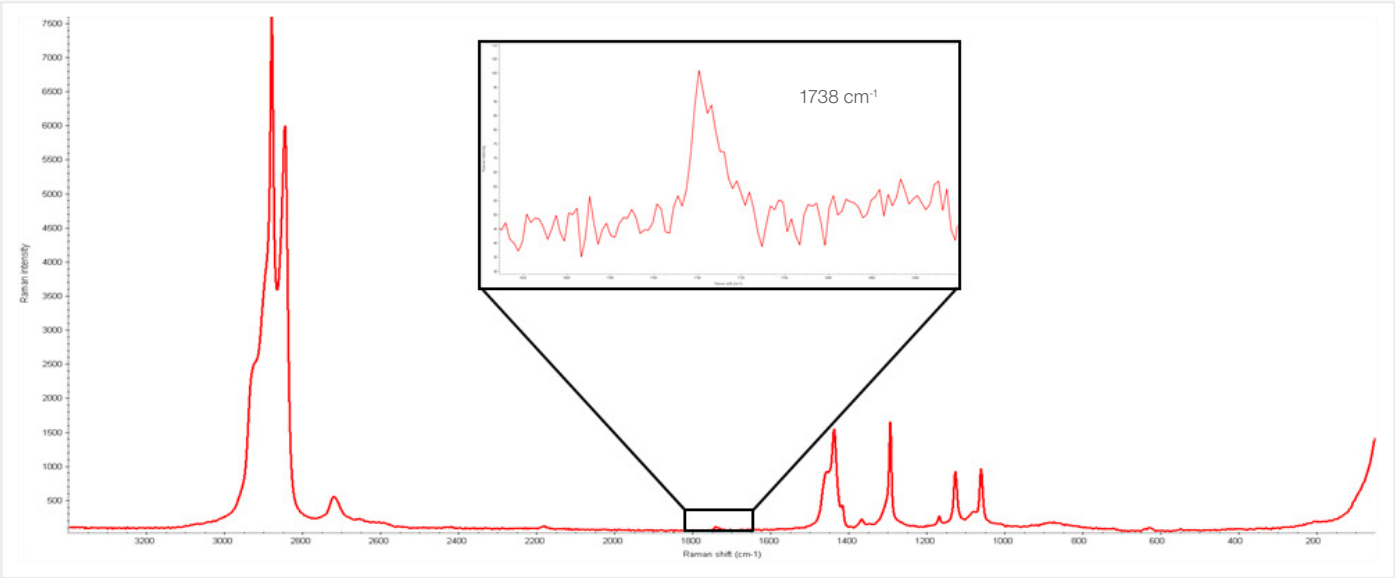

Figure 7. Acetate Carbonyl peak (1738 cm-1) in polymer layer #1.

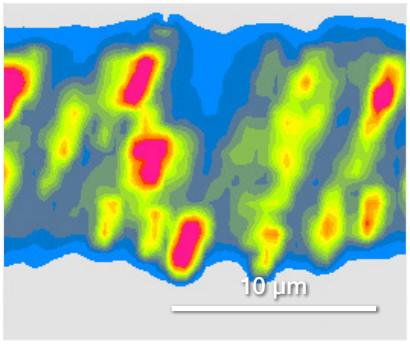

Raman Image showing the larger lazurite particles in layer 4 (red)

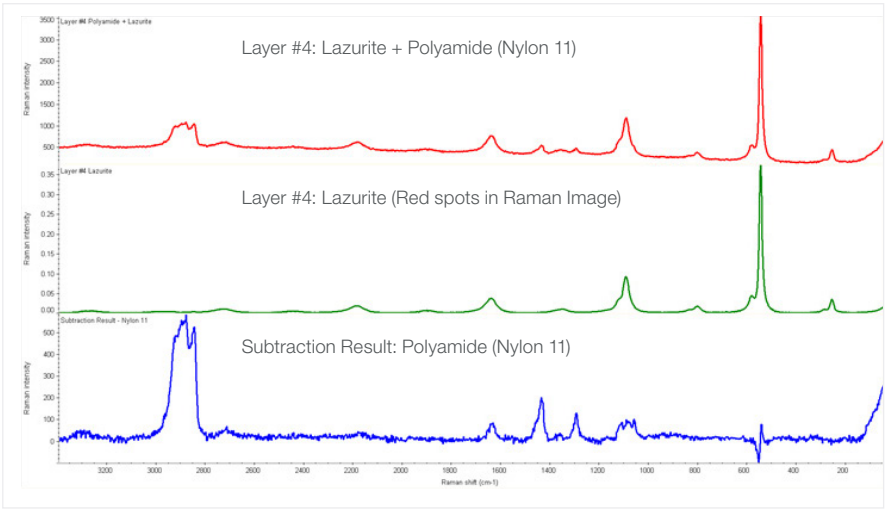

Figure 8. Particles of Lazurite in layer #4.

Conclusion

Whether the goal is quality assurance, failure analysis, or even reverse engineering of layered polymer composites, Raman and FTIR micro-spectroscopy are both valuable analytical tools for these types of applications. Imaging and mapping generates visual images depicting the distribution of the polymer components or variations in molecular structure.

Advantages & challenges of FTIR microscopy

1. Sensitive to polar functional groups found in many different types of polymers
2. Very useful for identifying different polymer types
3. Transmission analysis is a high throughput techniques but requires extensive sample preparation with the potential for sample deformations
4. ATR requires much less sample preparation and has the potential for higher spatial resolution but requires contact with the sample and possible sample deformation.

Advantages & challenges of Raman microscopy

1. Superior spatial resolution
2. Access to low wavenumber spectral range – great for identification of pigments
3. Requires very little sample preparation
4. Raman spectroscopy is very sensitive to molecular structure and highlights polymer backbones as opposed to polar functional groups.
5. Some polymer components and additives can show fluorescence that obscures Raman spectroscopy
6. In some cases highly focused laser sources may require lower power to avoid potential damage to the samples. A concerted approach utilizing both of these techniques provides for superior analysis of layered polymer composites because they support each other by addressing the shortcomings of the other technique and providing complementary information.

Morphological and chemical characterization of a non-woven fiber using electron and infrared microscopy

Authors

Matt Bartucci,[1] David Marchand,[2] and Rui Chen,[1] Antonis Nanakoudis[3]

[1]Thermo Fisher Scientific, Madison, WI, USA
[2]Nanoscience Instruments, Phoenix, AZ, USA*
[3]Thermo Fisher Scientific, Eindhoven, The Netherlands

*Authorized distributor of Thermo Scientific™ Phenom™ Microscope Systems.

Abstract

In this application note, the morphological and chemical characterization of a non-woven fiber sample is described. The SEM images suggest a fiber blend of at least two types of fiber, one of which has a possible sheath core structure. Through the library searching of the FTIR spectra, the non-woven fibers were determined to contain cellulose, PET and PE. The correlation profiles of the fibers confirm the presence of a sheath core structure, where the PET core is surrounded by the PE sheath.

Application benefit

The example demonstrates the complementarity between SEM and FTIR microscopy in material characterization: SEM excels in spatial resolution to understand materials' morphology, whereas FTIR microscopy offers molecular level insight into the underlying chemistry.

Our solutions

- Nicolet iN10 MX Imaging Infrared Microscope, OMNIC Software,
- Phenom ProX Desktop Scanning Electron Microscope

Thermo Scientific™ Phenom™ ProX Desktop Scanning Electron Microscope.

Thermo Scientific™ Nicolet™ iN10 MX Imaging Infrared Microscope.

Introduction

Non-wovens are one of the fastest-growing segments of the textile industry and constitute a significant portion of the fiber industry. Multi-layer non-woven composites, laminates, and three-dimensional non-woven fabrics are commercially produced and used in a wide variety of industrial engineering, consumer, and healthcare products. The complexity of these fibrous materials mandates the use of multiple analytical techniques for their full characterization.

Scanning electron microscopy (SEM) and Fourier transform infrared (FTIR) microscopy are two widely used microscopy techniques for the characterization of non-woven materials. Using electrons as the radiation source, SEM offers higher spatial resolution (in nm scale) than other optical techniques. The large depth-of-field of SEM also yields images with a characteristic three-dimensional appearance beneficial for understanding the surface structure of a sample. While the difference in chemical composition at elemental level is manifested by the contrast in SEM images, the exact chemical identity cannot be readily determined. On the other hand, by leveraging the spatial specificity of microscopy and the chemical specificity of spectroscopy, FTIR microscopy can provide molecular level chemical annotation to sample morphology. The spatial resolution of FTIR microscopy, however, is limited by the diffraction limit of the infrared light to approximately 10 µm. The combination of FTIR microscopy and desktop SEM can provide a holistic insight into materials' structure-function relationship from both the chemical and the morphological standpoints.

In this application note, the structural and chemical characterization of a non-woven fiber sample using both FTIR microscopy and desktop SEM is illustrated. While SEM allowed for a quick visual discernment of the different constituents in the sample, FTIR microscopy offered chemical identification of the constituents, and thereby shed light on the associated production process.

Experimental

Sample: The non-woven sample used in this study is an off-the-shelf hygiene wipe.

Fourier transform infrared microscopy: A bundle of non-woven fibers was isolated under a stereoscope and flattened with the back end of a roller knife onto an aluminum mirror. They were analyzed with the Thermo Scientific™ Nicolet™ iN10 MX Imaging Infrared Microscope using a 15X objective. Two images were acquired with a linear array detector and another one with a single-point MCT-A detector. Spectra on all maps were acquired in reflection mode with 16 scans co-added at a 16 cm^{-1} resolution.

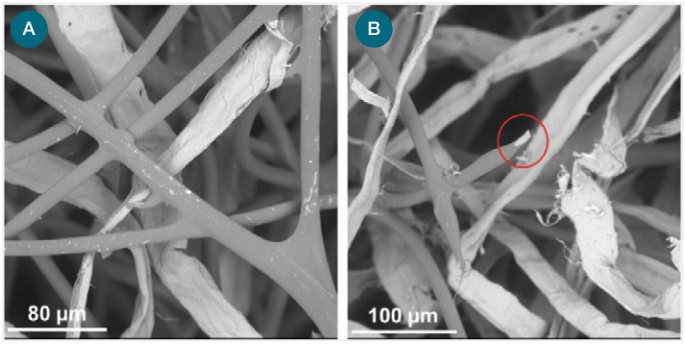

Figure 1. SEM images of (a) non-woven fiber bundle; and (b) an area where possible sheath core structure was observed (red circle).

Scanning electron microscopy: Images were acquired using a Thermo Scientific™ Phenom™ ProX Desktop Scanning Electron Microscope. A small piece of the nonwoven fibers was cut from the bulk sample and mounted onto a standard ½ inch pin-mount SEM stub using doublesided carbon tape. For the acquisition of the SEM images, the standard backscattered electron (BSE) detector of the Phenom ProX Microscope was utilized. The main contrast mechanism on such images is based on elemental differences. To maximize the elemental contrast of the organic samples, a relatively low electron beam voltage should be applied, which could result in lower quality images. However, due to the high-brightness electron source with which the Phenom ProX Desktop SEM is equipped, high-resolution images at 5 kV beam voltage were acquired without compromising their quality.

In this experiment, the inherent charge-reduction mode (low-vacuum operation) of the Phenom ProX Desktop SEM was utilized to prevent the non-conductive samples from charging. Using this approach combined with the advantage of the high-brightness electron source, sputter coating the sample with a metallic layer could be avoided, allowing investigation of the sample in its original form.

Results and discussion

Figure 1 shows the SEM images of two different sections of the fiber sample using a backscattered electrons (BSE) detector. Heavy elements (high atomic number) scatter electrons more strongly than light elements (low atomic number), and thus appear brighter in the image.

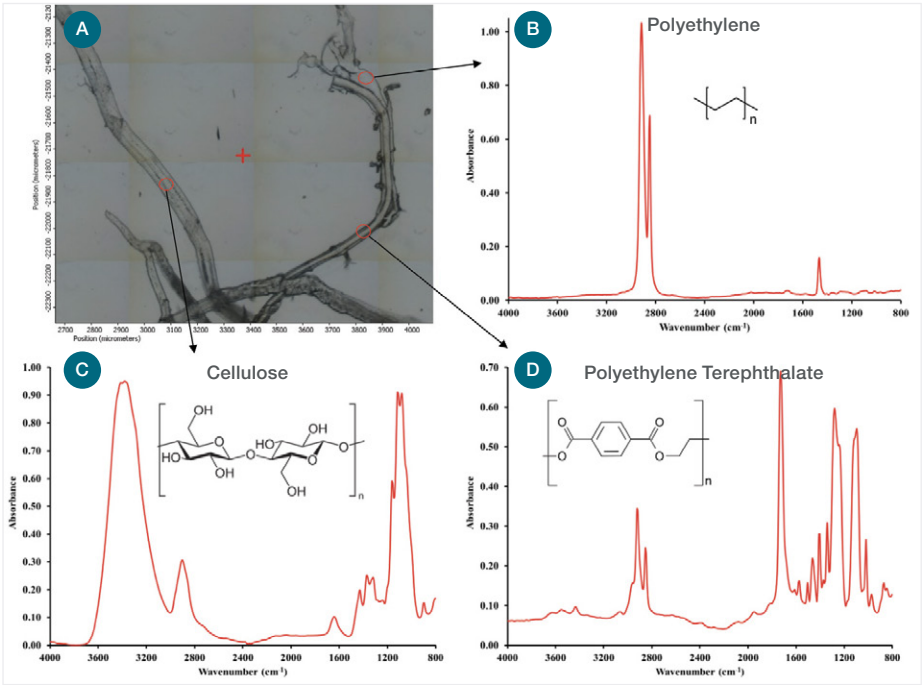

Figure 2. (a) Video image of the fibers obtained by Nicolet iN10 MX Microscope. Representative spectra and chemical structure of (b) polyethylene, (c) cellulose, and (d) polyethylene terephthalate. Red circles show the locations where the representative spectra were taken.

The contrast in the grayscale image signifies different chemical compositions. Figure 1a indicates that at least two types of fibers are present in the sample: one with smooth textures in dark color and one with wrinkled texture in white color. Closer examination (red circle in Figure 1b) further reveals that the dark-colored fibers are likely comprised of two different chemical compositions: a possible sheath core structure with a dark outer layer and a white inner core.

To investigate the chemical origins of the different types of fibers observed by SEM, the sample was analyzed by FTIR microscopy. Figure 2 shows the video image (approx. 1.2×1.5 mm) and the representative spectra taken at three different spots of the sample. A library search indicates that the selected spectra (Figures 2 b–d) match polyethylene (PE), cellulose and polyethylene terephthalate (PET), respectively.

The representative spectra shown in Figures 2 b–d were used as the reference spectra to construct the correlation profiles, wherein the red color represents a high degree of correlation, i.e., a greater similarity, with the respective reference spectra. Figure 3 shows the correlation images overlaid with the video images. Of particular interest is Figure 3c where a noticeable PE moiety resides adjacent to the PET fiber, supporting the hypothesis of a sheath core structure suggested by SEM (Figure 1b): a high melting point (~250 °C) PET core surrounded by a low melting-point (~120 °C) PE sheath. During production when the fibers are heated, the sheath layer melts and adheres to each other at the junctions. A crosslinking network is formed to achieve the desired mechanical strength while maintaining the structural integrity.

Conclusions

This application note describes the characterization of a non-woven fiber sample. The contrast in the SEM images suggests a fiber blend of at least two types of fiber, one of which has a possible sheath core structure. FTIR microscopy provides corroborating evidence from the chemistry perspective to support the observations by SEM. Through the library searching of the FTIR spectra, the non-woven fibers were determined to contain cellulose, PET and PE. The correlation profiles of the fibers confirm the presence of a sheath core structure, where the PET core is surrounded by the PE sheath. The example clearly demonstrates the complementarity between SEM and FTIR microscopy in material characterization: SEM excels in spatial resolution to understand materials' morphology, whereas FTIR microscopy offers molecular level insight into the underlying chemistry. The great analytical power unleashed from the combination of these two microscopy techniques should be welcomed by those in research and development as well as quality control/quality assurance across many industries.

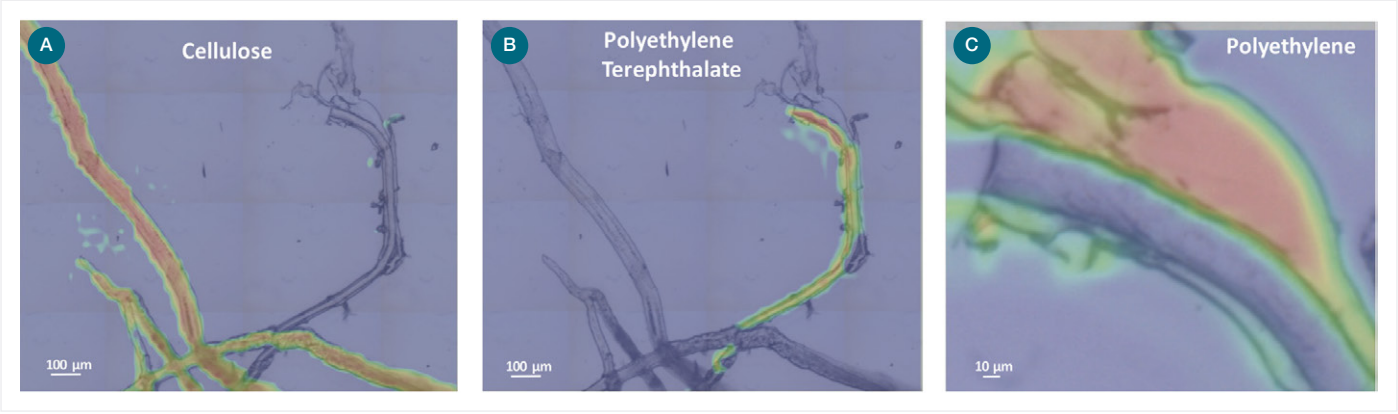

Figure 3. Chemical correlation maps overlaid with video image of fibers. Correlation maps correspond to where (a) cellulose, (b) polyethylene terephthalate and (c) polyethylene are located across the visual image.

Learn more about the **Thermo Scientific Phenom ProX G6 Desktop SEM**
Learn more at **thermofisher.com/in10mx**

In situ density determination of polyethylene in multilayer polymer films using Raman microscopy

Authors

Mohammed Ibrahim, Ph.D.
Herman He, Ph.D. and Rui Chen, Ph.D.
Thermo Fisher Scientific
Madison, WI, USA

Keywords

Polyethylene (PE), density, Raman Microscopy, DXR2 Raman Microscope, Partial Least Squares (PLS)

Application benefits

Polyethylene density determination based on Raman microscopy and Partial Least Squares (PLS) regression is applicable for both pellet and film samples. The confocal capability of Raman microscopy allows for *in situ* density determination of PE layers within multilayer polymer films, without the need for tedious and challenging sample preparations.

Thermo Fisher Scientific solutions

- Thermo Scientific™ DXR2 Raman Microscope
- Thermo Scientific™ OMNIC™Software
- Thermo Scientific™ TQ Analyst™Software

Introduction

Polyethylene (PE) is one of the most common plastics in the world with an annual global production of around 80 million tons.[1] Unlike other commercial polymers, PE can be manufactured across a range of densities that are related to the spacing between the polymer chains.[2] For examples, High-Density PE (HDPE, 0.941-0.965 g/cm^3) is mainly comprised of linear PE chains that can closely approach each other, thus creating very densely packed networks. Conversely, Low-Density PE (LDPE, 0.910-0.940 g/cm^3) has excessive branching that causes a less compact molecular structure. Linear Low-Density PE (LLDPE, <0.940 g/cm^3), too, has a large number of branches, but the branches are shorter than those in LDPE. Because the density of PE can be controlled and varied, it provides an important mechanism to control its properties to suit different applications. PE density is therefore a vital part of the material characterization and selection process.

There are several standard methods for PE density measurement, such as ISO 1183-1/ASTM D792 (immersion method)[3], ISO 1183-2/ASTM D1505 (density gradient method),[4] and ASTM D4883 (ultrasound method)[5]. These methods, however, are primarily geared towards PE samples in a “pure” form such as pellets and single-layer films. Challenges arise when PE is present in multilayer films, which are widely used in food, pharmaceutical and consumer product packaging. Extensive sample preparations, including microtoming and separation of layers using solvents, are required to isolate the PE layer(s) before analysis, which can be labor-intensive and time-consuming.[6]

Thermo Scientific DXR2 Raman Microscope.

To that end, Raman microscopy could offer an *in situ* density determination of PE layers in multilayer films by leveraging its confocal capability. Raman spectroscopy has long been utilized to investigate the structure of polymers, including molecular conformation, orientation, and crystal structure.[7-9] Combined with multivariate analyses such as principal component analysis (PCA) and partial least squares (PLS) regression whereby statistically observed spectral variations are correlated with known sample properties, crystallinity, density and melting point can be predicted.[7] Existing literature, however, has also been limited to bulk PE pellets. In our previous report,[10] we expanded the scope of the methodology to include PE films. It is demonstrated that Raman microscopy in combination with a PCA based discriminant analysis can qualitatively distinguish HDPE and LDPE in both pellet and film forms. In this application note, we will describe the development of a Partial Least Squares (PLS) model to quantitatively determine the density of PE layers in both single-layer and multilayer films using Raman microscopy.

Experimental

A total of 25 PE samples (12 pellets and 13 films) with different known densities (Table 1) were used for developing a PLS model for density determination. All samples were used as received. A clear transdermal nicotine patch sample was used for identifying the PE layers and *in situ* determination of PE layer densities. The sample was mounted onto a gold-coated microscope slide with the backing layer facing the microscope objective, and the release liner at the bottom.

A Thermo Scientific™ DXR2™ Raman Microscope was used for collecting Raman data. For each of the pellet samples, Raman spectra were collected from 3 different pellets and averaged. For each of the film samples, Raman spectra were collected from 3-4 locations across the surface of the sample. An averaged spectrum was then used for final analysis. A 532 nm laser was used with 2 mW laser power at the sample. A 10x objective and a 50 µm slit aperture were used to obtain more representative spectra from the samples. Total acquisition time for each spectrum was 30 seconds (3 second exposure x 10 exposures). For the transdermal nicotine patch sample, Raman confocal line depth profiling was performed using a 532 nm laser, 5 mW laser power at the sample, 50x objective, 25 µm confocal pinhole aperture, and with auto exposure (S/N = 200). A depth of 220 µm was probed by using a 5 µm step size (containing 45 points or spectra).

Thermo Scientific™ OMNIC™ software was used for instrument control and data acquisition. Thermo Scientific™ TQ Analyst™ software was used for chemometric analysis of the Raman data.

Results and discussion

Raman spectra of HDPE, LDPE, and LLDPE

Representative Raman spectra of HDPE, LDPE, and LLDPE samples are shown in Figure 1. There are noticeable differences among three types of PE samples in both CH stretching (2900-3100 cm^{-1}) and CH_2 bending and twisting (1250-1500 cm^{-1}) regions. The intensity of the symmetric CH_2 stretching mode at 2848 cm^{-1} (relative to the asymmetric CH_2 stretching mode at 2882 cm^{-1}) decreases in the order of LLDPE > LDPE > HDPE (Figure 1A). In the CH_2 bending and the CH_2 twisting region (Figure 1B), the intensity of the CH_2 bending mode at 1416 cm^{-1} (relative to the CH_2 bending mode at 1440 cm^{-1}) is higher for HDPE than for LDPE. The 1416 cm^{-1} peak is completely absent for the LLDPE film sample (#19). This observation agrees with the previous reports that the 1416 cm^{-1} and 1440 cm^{-1} peaks are indicators of crystalline and amorphous PE phases, respectively.[7,8] The higher the crystallinity, the higher the density. Since the CH_2 bending region (1400-1500 cm^{-1}) is sensitive to the density of PE, it was selected for subsequent quantitative analysis.

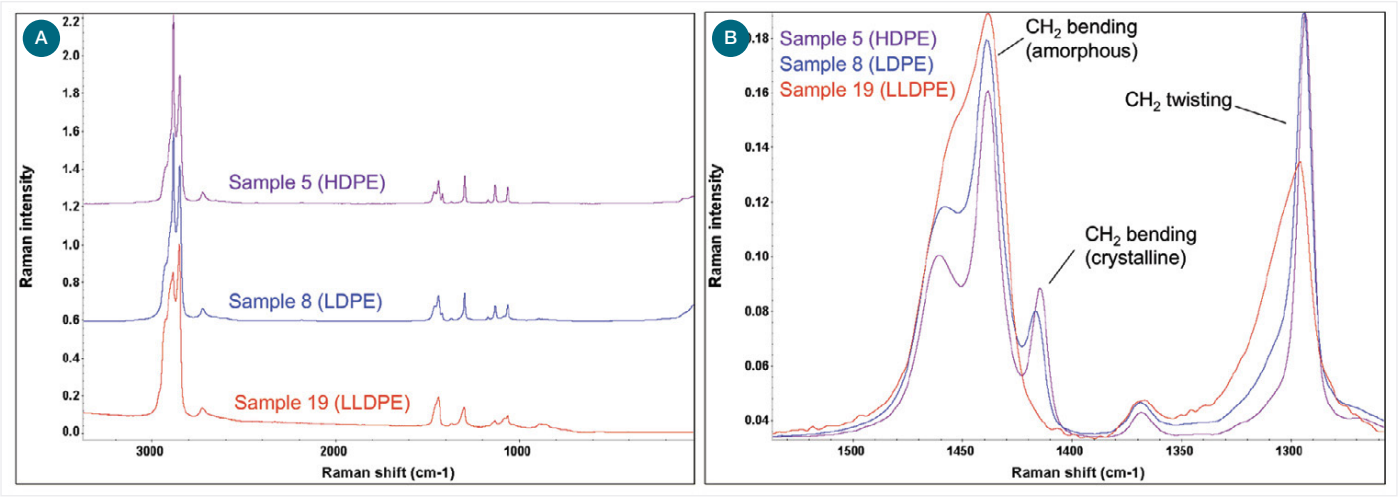

Figure 1. Representative Raman spectra of HDPE, LDPE, and LLDPE samples. (A) Full spectral range in stack view. (B) CH_2 bending and CH_2 twisting region in overlay view.

Data processing

Peak area for pathlength correction option in the TQ Analyst software was used to normalize Raman spectral intensities. The peak area of the CH_2 bending mode at 1440 cm^{-1} was used for the normalization (1422-1452 cm^{-1} range, Figure 2A). An averaged two-point baseline correction was used to account for baseline shifts/noise.

Developing a PLS model for PE density determination

Partial Least Squares (PLS) algorithm[11] from the TQ Analyst software was used to develop a model for PE density determination. PLS is a quantitative regression algorithm through statistical analysis. It uses spectral covariance and factorial analysis to extract significant and relevant chemical information from sample spectra as factors, then correlate them with sample properties such as concentration, crystallinity and density. A total of 20 samples, a mix of pellets and films, were used as the calibration standards. Five additional pellet and film samples with density values spread across the density range of the samples were selected as the validation standards (Table 1). A spectral range of 1400-1500 cm^{-1} with averaged two-point correction for baseline (Figure 2B) was used in the method.

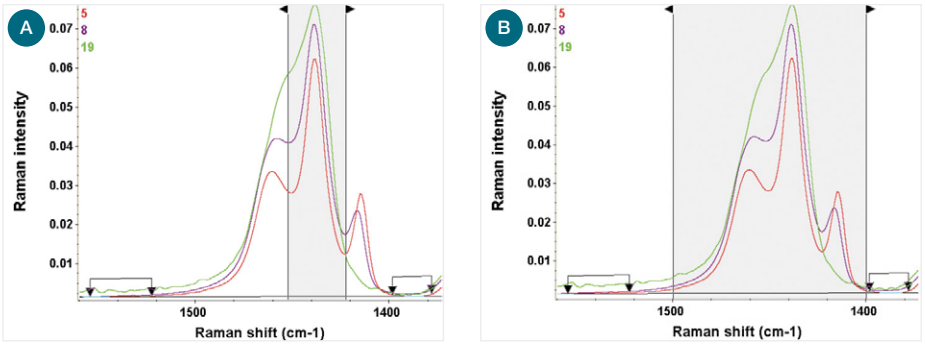

Figure 2. (A) Peak Area Ratio to normalize Raman spectral intensities, showing the CH_2 bending peak region for normalization. (B) Spectral range used for PLS calibration. In both cases, an averaged two-point option was used for baseline correction.

	Sample #	Actual density (g/cm^3)	PE Type	Usage	Calculated density (g/cm^3)	Difference (g/cm^3)	% Difference
Pellets	1	0.9460	HDPE	Calibration	0.9454	0.0006	0.06%
	2	0.9505	HDPE	Calibration	0.9486	0.0019	0.20%
	3	0.9510	HDPE	Calibration	0.9509	0.0001	0.01%
	4	0.9470	HDPE	Validation	0.9523	-0.0053	-0.56%
	5	0.9620	HDPE	Calibration	0.9564	0.0056	0.58%
	6	0.9600	HDPE	Calibration	0.9594	0.0006	0.06%
	7	0.9195	LDPE	Calibration	0.9236	-0.0041	-0.45%
	8	0.9170	LDPE	Calibration	0.9183	-0.0013	-0.14%
	9	0.9235	LDPE	Calibration	0.9250	-0.0015	-0.16%
	10	0.9300	LDPE	Calibration	0.9264	0.0036	0.39%
	11	0.9235	LLDPE	Calibration	0.9295	-0.0060	-0.65%
	12	0.9185	LLDPE	Calibration	0.9259	-0.0074	-0.81%
Films	13	0.9496	HDPE	Calibration	0.9568	-0.0072	-0.76%
	14	0.9606	HDPE	Calibration	0.9556	0.0050	0.52%
	15	0.9460	HDPE	Calibration	0.9456	0.0004	0.04%
	16	0.9247	LDPE	Calibration	0.9225	0.0022	0.24%
	17	0.9258	LDPE	Calibration	0.9241	0.0017	0.18%
	18	0.9297	LDPE	Calibration	0.9276	0.0021	0.23%
	19	0.8598	LLDPE	Calibration	0.8604	-0.0006	-0.07%
	20	0.8650	LLDPE	Calibration	0.8623	0.0027	0.31%
	21	0.8881	LLDPE	Validation	0.8812	0.0069	0.78%
	22	0.9008	LLDPE	Calibration	0.8993	0.0015	0.17%
	23	0.9040	LLDPE	Validation	0.9072	-0.0032	-0.35%
	24	0.9236	LLDPE	Validation	0.9215	0.0021	0.23%
	25	0.9367	LLDPE	Validation	0.9349	0.0018	0.19%

*Rows highlighted in green are the samples used for validation.

Table 1. PE samples and their densities.

Figure 3 shows the calibration results for PE densities obtained with the 3-factor PLS model. The inset is the Predicted Residual Error Sum of Squares (PRESS) plot. In the current case, a 3-factor model suffices as the contribution from the 4th and 5th factors are negligible. The calibration curve has a correlation coefficient of 0.9914. The RMSE (Root Mean Square Error) values are 0.00360 for the calibration samples and 0.00432 for the validation samples, respectively. The results are also summarized in Table 1. For all 25 samples, the calculated densities are within ±0.81% of the actual values.

It is important to note that the percent differences do not exhibit any bias between pellets and films, indicating that the sample form (pellets vs. films) has no bearing on the model performance.

Density determination of PE films

Figure 4 demonstrates an example of applying the Raman spectrum and the PLS model to predict the density of a PE film sample. The predicted density is 0.9014 g/cm^3, showing a good agreement with the actual density of 0.9008 g/cm^3.

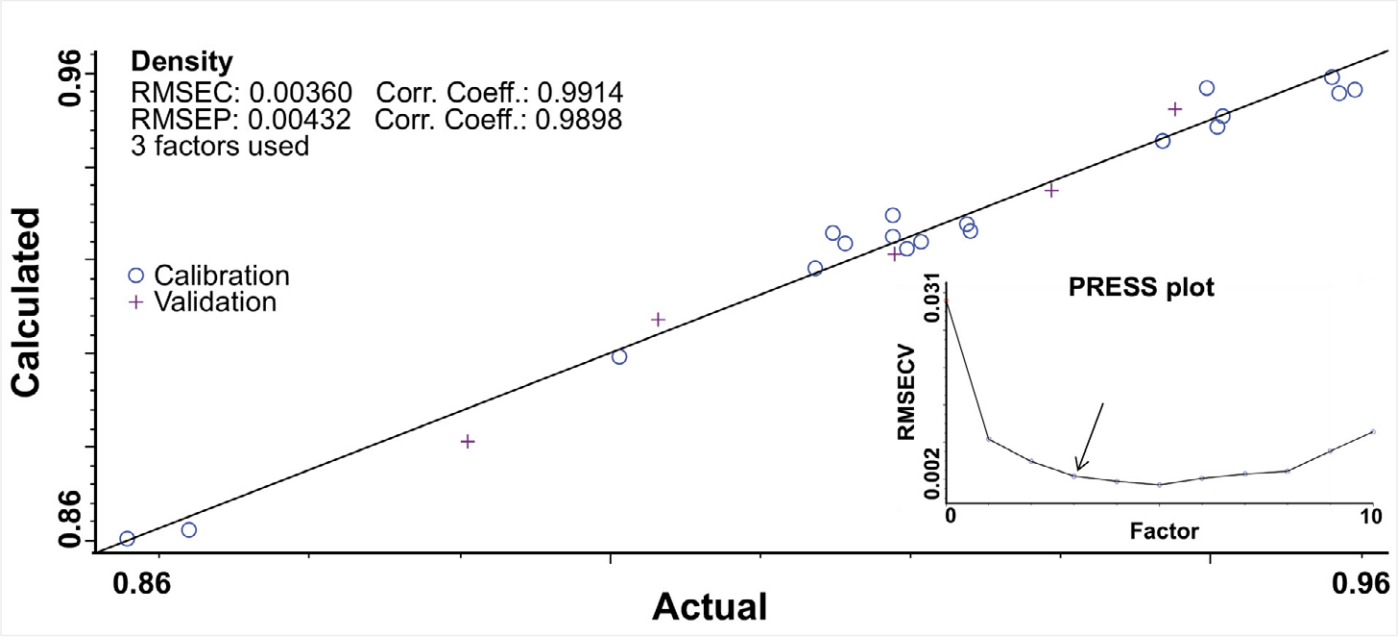

Figure 3. Calibration results for PEs of different densities using a PLS quantitative analysis. The denotes calibration standards and the + denotes validation standards. Inset is the PRESS plot for the PLS calibration. Three factors were used in the current PLS calibration model.

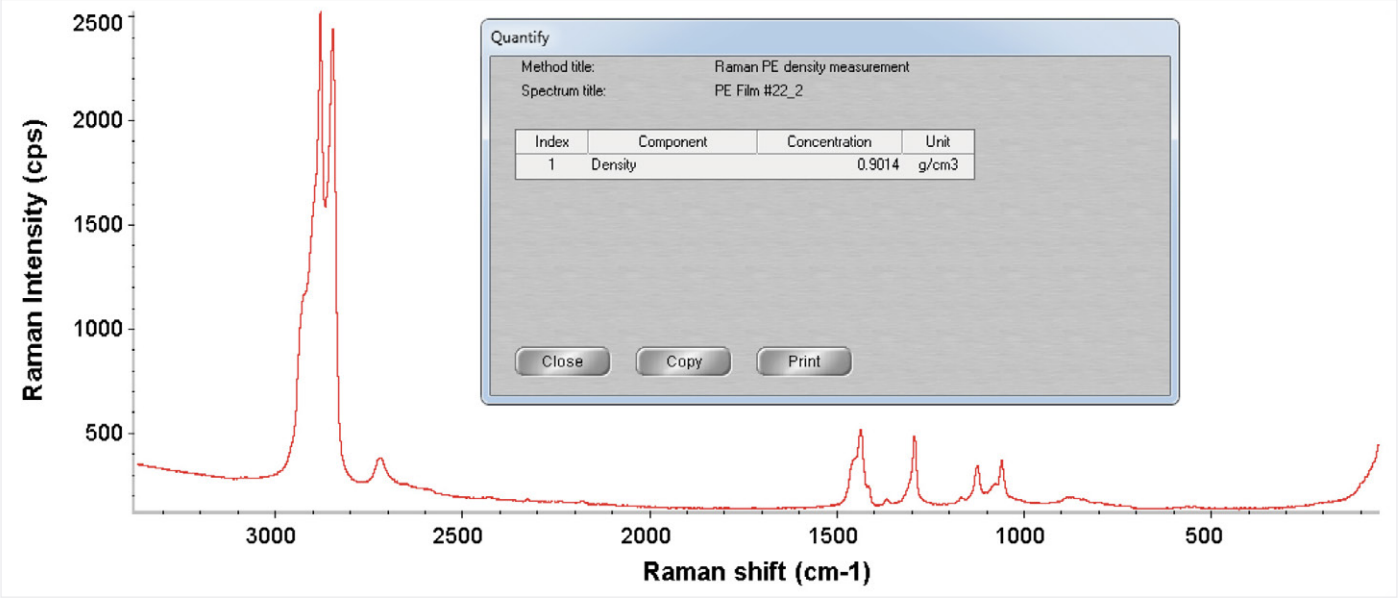

Figure 4. Prediction of the density of a PE film sample using its Raman spectrum and the PLS model. The known density of the film is 0.9008 g/cm^3 and the predicted density is 0.9014 g/cm^3.

Figure 5A shows the Raman confocal depth profile of a clear transdermal nicotine patch. A total of 6 polymer layers were identified, including two PE layers – PE layer 1 (part of the backing layer) and PE layer 2 (closer to the release liner). There are perceptible differences in the Raman spectra between the two PE layers (Figure 5B and 5C). Applying the PLS model, the densities are determined to be 0.9150 g/cm3 for PE Layer 1 and 0.9583 g/cm^3 for PE Layer 2, placing PE layer 1 in the LDPE /LLDPE class and the PE Layer 2 in the HDPE class. The classification of the PE layers based on the predicted densities conforms to other reports: LDPE/LLDPE is used in the occlusive backing layer for its flexibility whereas HDPE is used as the rate-controlling membrane as an integral part of the reservoir diffusion control machanism.[12-13] While the exact densities of the two PE layers are not available, the results presented here nonetheless demonstrates the advantage of using Raman microscopy combined with the PLS method for density determination. The confocal capability of Raman microscopy allows for *in situ* PE density determination in multi-layer films without the need to isolate the individual PE layers.

Conclusions

Raman microscopy is a powerful analytical tool for PE density determination. Since PE chains in crystalline and amorphous domains exhibit unique Raman features in the CH_2 bending region, a PLS model based on the Raman features in the 1400-1500 cm^{-1} region was successfully developed. The model is applicable for both pellet and film samples, showing a good agreement between actual and predicted density values. Applying the model to a real-world multilayer film containing two PE layers, the predicted density values correctly place the two layers into their respective PE classes. More importantly, the confocal capability of Raman microscopy allows for *in situ* density determination of PE layers within multilayer polymer films, without the need for tedious and challenging sample preparations required by many other techniques. The presented methodology should be of interest for PE manufacturers as well those who perform failure analysis, reverse engineering, and polymer composites development.

Acknowledgement

The authors would like to thank Wanda Weatherford at Chevron Phillips Chemical Company for providing PE pellet samples and Rajesh Paradkar at Dow Chemical Company for providing PE film samples.

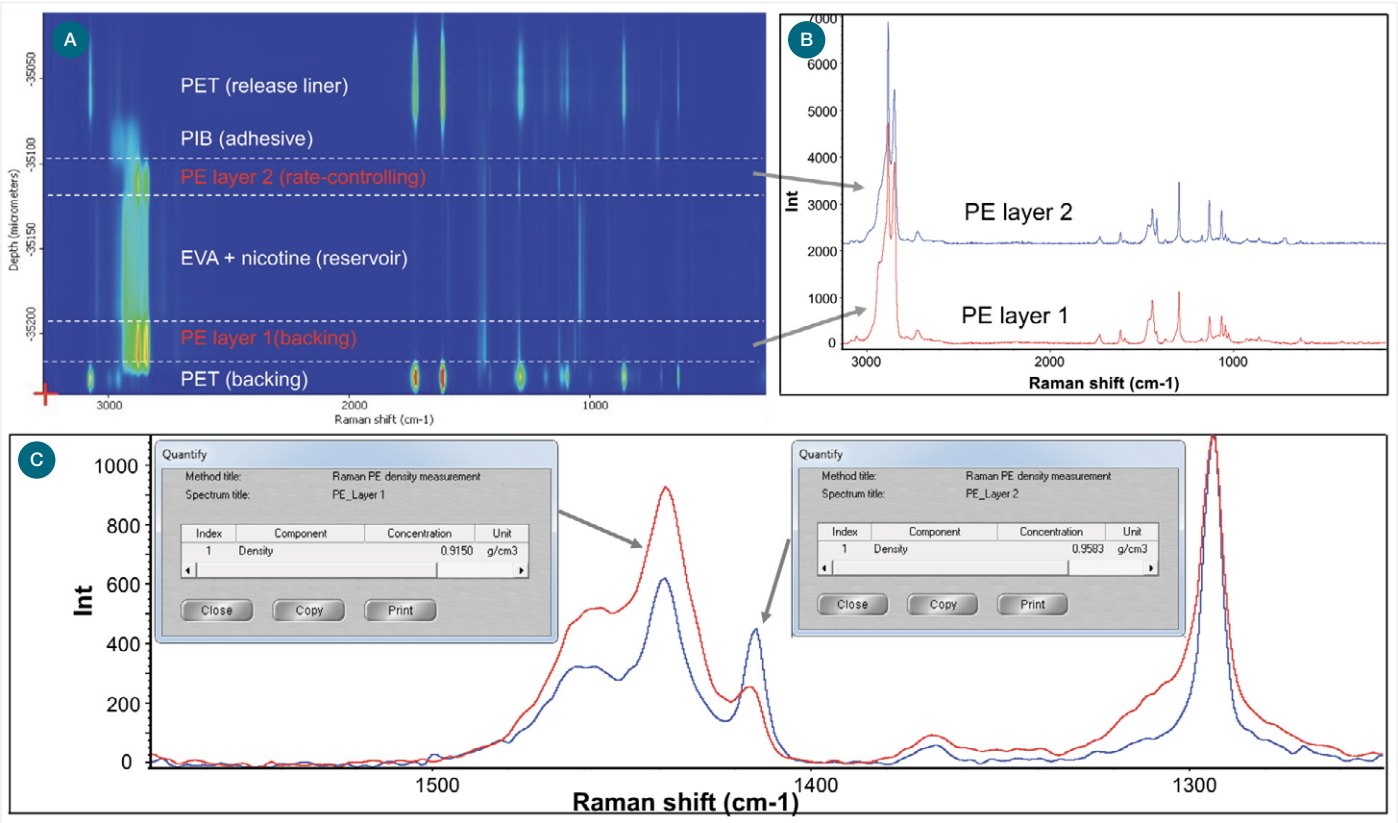

Figure 5. (A) Confocal Raman line depth map of a multilayer polymer patch, showing the presence of two types of PE layers. (B) Raman spectra of the two PE layers in full spectral range. (C) Raman spectra of the two PE layers in the CH_2 bending and CH_2 twisting region. The insets in (C) show the calculated densities of the two PE layers using the 3-factor PLS model. PET = poly(ethylene terephthalate), EVA = ethylene/vinyl acetate copolymer, PIB = polyisobutylene.

References

1. Piringer O.G. and Baner A.L., ed. Plastic Packaging: Interactions with Food and Pharmaceuticals. 2nd ed. Weinheim: Wiley-VCH; 2008.
2. Polyethylene, The Essential Chemical Industry – online, *essentialchemicalindustry.org/polymers/polyethene.html*, retrieved on 11/27/2017.
3. (a) ISO 1183-1:2012, Plastics – Methods for determining the density of non-cellular plastics – Part 1: Immersion method, liquid pyknometer method and titration method; ANSI New York, NY. (b) ASTM D792-13, Standard test methods for density and specific gravity (relative density) of plastics by displacement; ASTM International, West Conshohocken, PA, 2013.
4. (a) ISO 1183-2:2004, Plastics – Methods for determining the density of non-cellular plastics – Part 2: Density gradient column method. ANSI New York, NY. (b)ASTM D1505-10, Standard test method for density of plastics by the density-gradient technique; ASTM International, West Conshohocken, PA, 2010.
5. ASTM D4883-08, Standard test method for density of polyethylene by the ultrasound technique; ASTM International, West Conshohocken, PA, 2008.
6. Mieth A., Hoekstra E., and Simoneau C. Guidance for the identification of polymers in multilayer films used in food contact materials: User guide of selected practices to determine the nature of layers, EUR 27816 EN, 2016; doi: 10.2788/10593.
7. Sato H., Shimoyama M., Kamiya T., Amari T., Sasic S., Ninomiya T., Siesler H.W., and Ozaki Y. Raman spectra of high-density, low-density, and linear low-density polyethylene pellets and prediction of their physical properties by multivariate data analysis, J. Appl. Polym. Sci., 2002, 86, 443–448.
8. Strobl G.R. and Hagedorn W. Raman spectroscopic method for determining the crystallinity of polyethylene, J. Polym. Sci. B Polym. Phys., 1978, 16, 1181-1193.
9. Williams K.P.J. and Everall, N. J. Use of micro Raman spectroscopy for the quantitative determination of polyethylene density using partial least-squares calibration, J. Raman Spectrosc. 1995, 26, 427-433.
10. Ibrahim M. and He H. Classification of polyethylene by Raman spectroscopy, Thermo Scientific Application Note AN52301, 2017.
11. Thermo Scientific Product Overview. TQ Analyst Software Chemometric Algorithms, 2009.
12. Kearney C. J. and Mooney D.J. Macroscale delivery systems for molecular and cellular payloads, Nat. Mater., 2013, 12, 1004-1017
13. Allen L. V. and Ansel H. C., ed. Ansel's Pharmaceutical Dosage Forms and Drug Delivery Systems, 10th ed. Lippincott Williams & Wilkins; 2013.

Characterization of Contaminants in Recycled PET and HDPE using FTIR Microscopy

Authors

Suja Sukumaran, PhD,
and Rui Chen, PhD,
Thermo Fisher Scientific

Introduction

Reducing environmental pollution and energy consumption in recycling are the paramount driving forces behind research on recycling plastics. The advances in reclamation technologies have pushed the boundaries of recycled plastics or post-consumer resin (PCR) use to include many high-end applications such as food packaging, electronics, and automobiles. These applications often demand near-prime qualities of any recycled plastics. Furthermore, as more and more countries across the globe ban the use of single use plastics, there has been a steady increase in the demand for PCR over virgin resins. To ensure the performance and aesthetic quality of recyclates in second-market applications, it is imperative that fast, reliable, and cost-effective characterization and quality control procedures are implemented at different stages of recycling and manufacturing operations.[1]

The challenges in large-scale use of recyclates in the second-market plastic manufacturing arise from the unknown origins of the feedstock, the presence of any contaminants, and possible degradation during previous usage. Traditionally, bulk properties such as melt flow rate and mechanical properties have been used to assess the quality of the recyclates. These macroscopic properties, however, are only indirectly correlated to materials' underlying chemistry and cannot identify contaminants. To that end, FTIR microscopy can provide a more holistic understanding of the material at molecular level by annotating sample morphology with chemical information.

In this application note, we demonstrate the use of FTIR microscopy for the characterization of recycled polyethylene terephthalate (PET) and polyethylene (PE) PCRs. The results show that cellulosic fragments are common contaminants in recycled polymers. Depending on the morphology of the contaminants, different sampling techniques should be adopted for the analysis.

Materials and methods

FTIR microscopy was carried out using a Thermo Scientific™ Nicolet™ iN10 MX Infrared Imaging Microscope. Three modes of analysis were used: reflection, transmission and micro ATR (µ-ATR). These were applied across different types of sample sets.

For the PET powder sample, an area map was collected in reflectance mode. The PET powders were spread onto a gold slide and analyzed without further sample preparation. The XY area map was collected using an MCT-A detector, 50 µm spatial resolution, and 8 scans at 8 cm^{-1} spectral resolution at each map point.

For the analysis of the PE pellets, particles were first isolated from the surface of the pellets under a preparatory microscope at 3× magnification. Isolated particles were then placed onto a glass slide and analyzed in ATR mode. A slide-on germanium (Ge) tip ATR was used for the analysis of the isolated contaminant particles. An MCT-A detector was used for all samples, and 64 scans at 4 cm^{-1} resolution were collected in 22 seconds for each spectrum. The Ge crystal tip was cleaned between sample analyses using 70% isopropanol.

A grocery bag sample was analyzed as received. A small piece of the grocery bag sample was cut, placed on a transmission holder, and analyzed in transmission mode. An area map with a spatial resolution of 50 µm was collected, using 4 scans at 8 cm^{-1} spectral resolution at each XY map point.

Results and discussion

Characterization of recycled PET powders by reflectance FTIR microscopy

Polyethylene terephthalate (PET) accounts for approximately 10% of the plastic produced worldwide and is extensively used for single use bottle packaging. Figure 1 summarizes the reflectance FTIR microscopy experiments of the recycled PET powders. An area of approximately 2.5×2.5 mm^2 was mapped, in which the PET particles range from tens to hundreds of micrometers in dimension. There are noticeable fibrous features in the optical image (Figure 1A). The FTIR spectrum of the particles (Figure 1C) shows a positive match to PET. The PET spectrum was then used as the reference spectrum for correlation profiling, and the resulting correlation map was superimposed with the optical image (Figure 1B); the warm color indicates a high degree of correlation. Major peaks characteristic to PET, such as 1710 cm^{-1} (the C=O stretching), 1241 cm^{-1} and 1094 cm^{-1} (the C-O stretching), 844 cm^{-1} (trans CH_2 rocking) and 723 cm^{-1} (the aromatic C-H out-of-plane bending), are observed in both the sample spectrum (red) and reference spectrum (blue). Note that the peak at 3430 cm^{-1}, attributed to the hydroxyl groups, shows a higher relative intensity in the recycled PET. The chain scissions during PET recycling could generate polymer radicals with hydroxyl groups.[2]

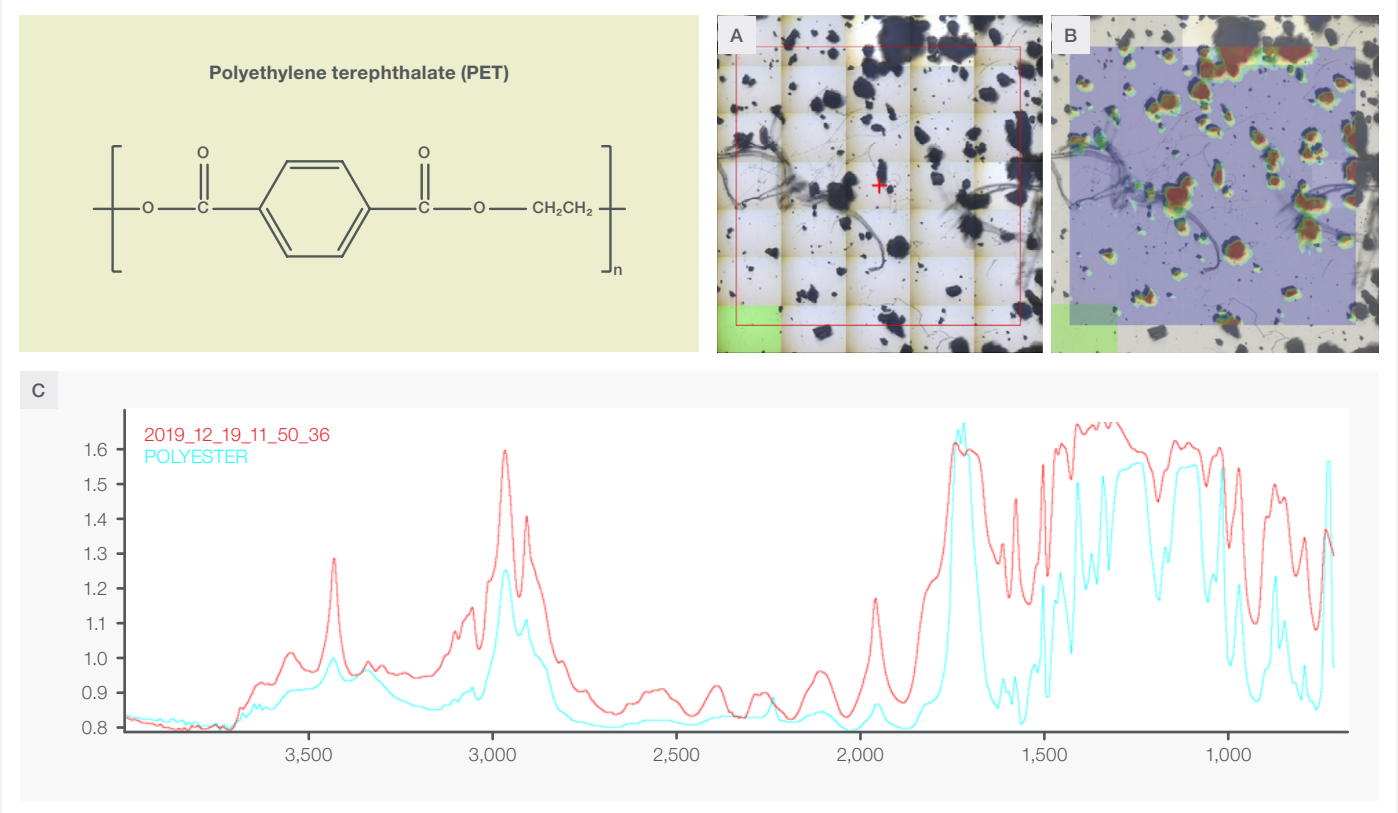

Figure 1. Analysis of recycled PET powders using reflectance FTIR microscopy. (A) Optical image of the recycled PET powders spread on a gold slide. (B) Chemical image superimposed with the optical image. The chemical image is the correlation profile using the PET spectrum as the reference. (C) Reflectance FTIR spectra of the recycled PET particles (red) and the standard reference spectrum from the library (blue).

The same procedure was repeated for the fibrous features observed in the optical image (Figure 2A). The resulting spectrum (Figure 2C) shows a positive match to cellulose. The observed peaks in the spectral range of 3600 - 2900 cm^{-1} are characteristic for the stretching vibrations of the O-H and C-H bonds in polysaccharides: the band at ~2900 cm^{-1} is attributed to the C-H stretching vibration of the hydrocarbon constituent, and the broad peak centered at 3300 cm^{-1} is ascribed to the stretching vibration of the hydroxyl group, including both inter- and intra-molecular hydrogen bond vibrations. In the fingerprint region, the peaks located at ~1640 cm^{-1} correspond to the vibration of water molecules absorbed in cellulose. The absorption bands at 1428, 1367, 1334, 1027 and 896 cm^{-1} arise from stretching and bending vibrations of $-CH_2$ and -CH, -OH and C-O bonds in cellulose.[3] Cellulose is mainly used to produce paperboard and paper and therefore it is a common contaminant found in recycled polymers, possibly originating from labels and stickers on many consumer products. Cellulosic contaminants are undesirable as they can be cascaded into the end products, negatively affecting the products' performance and aesthetic.

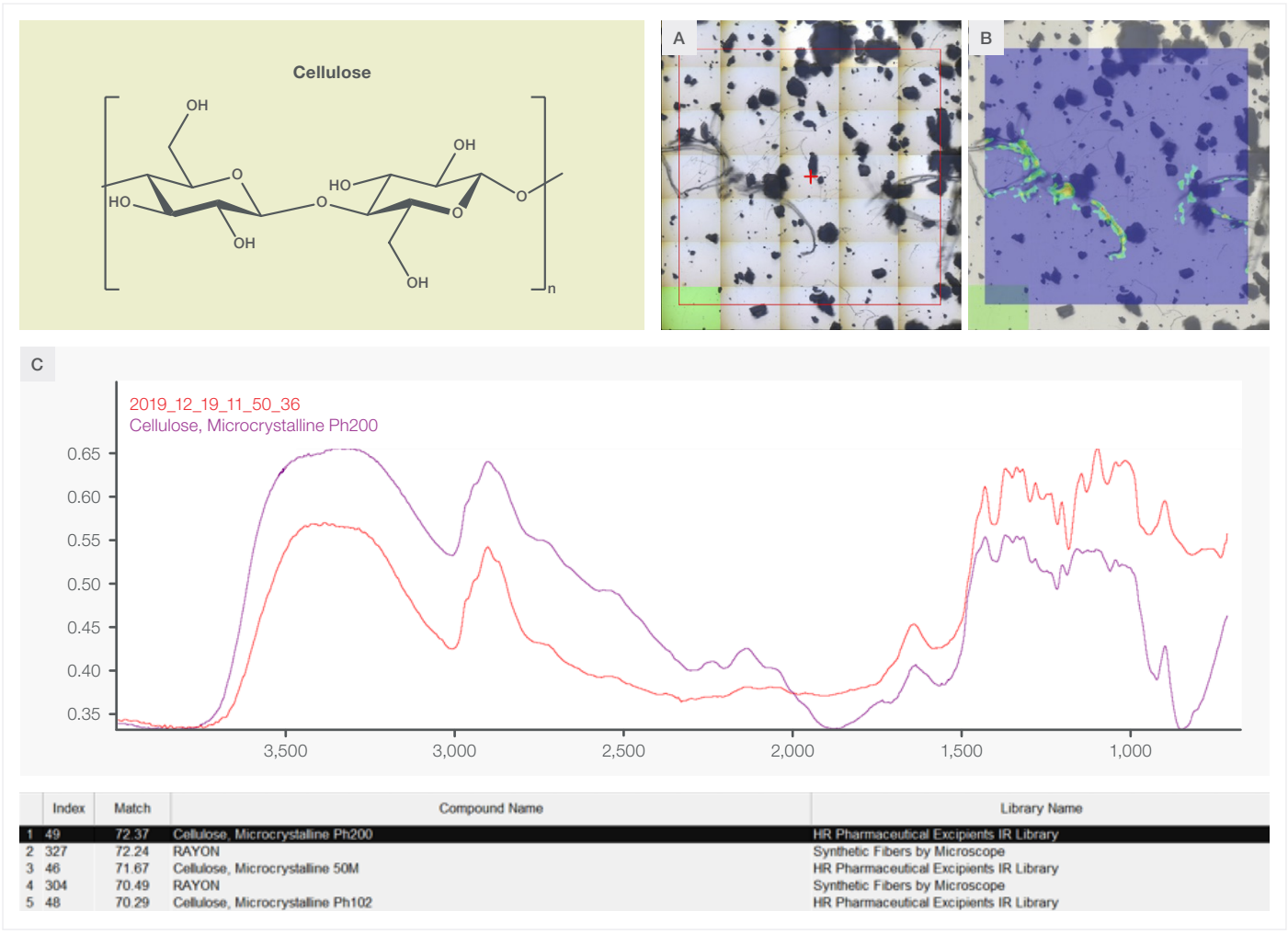

	Index	Match	Compound Name	Library Name
1	49	72.37	Cellulose, Microcrystalline Ph200	HR Pharmaceutical Excipients IR Library
2	327	72.24	RAYON	Synthetic Fibers by Microscope
3	46	71.67	Cellulose, Microcrystalline 50M	HR Pharmaceutical Excipients IR Library
4	304	70.49	RAYON	Synthetic Fibers by Microscope
5	48	70.29	Cellulose, Microcrystalline Ph102	HR Pharmaceutical Excipients IR Library

Figure 2. Analysis of the fibers in the recycled PET powders using reflectance FTIR microscopy. (A) Optical image of the recycled PET powders spread on a gold slide. (B) Chemical image superimposed with the optical image. The chemical image is the correlation profile using the cellulose spectrum as the reference. (C) Reflectance FTIR spectrum of the cellulose fibers (red) and the standard reference spectrum from the library (purple).

Analysis of the contaminants in recycled HDPE pellets by ATR FTIR microscopy

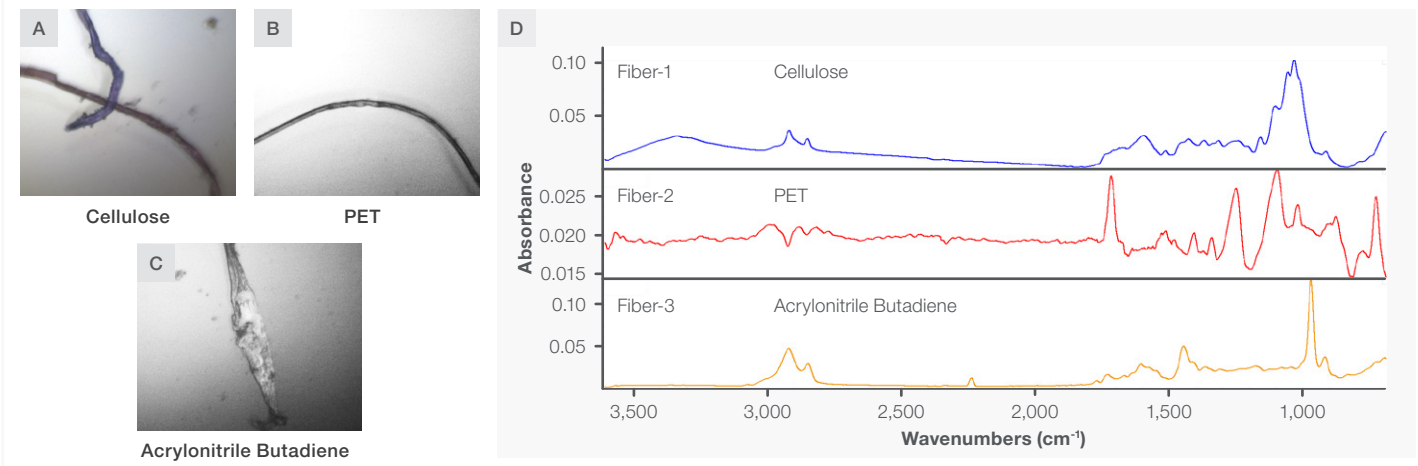

Figure 3. µ-ATR FTIR microscopy of recycled PE pellets.

The FTIR microscopic analysis shows that there are at least three types of fibers present in the recycled HDPE pellets: cellulose (Figure 3A), PET (Figure 3B) and acrylonitrile butadiene (Figure 3C). The representative FTIR spectra of the three types of fibers are shown in Figure 3D, where the fibers can be readily differentiated.

In the same pellet sample, there are visually discernible black particles (insert of Figure 4). The particles were isolated from the pellet and subjected to µ-ATR FTIR microscopy analysis. The results are shown in Figure 4. Upon library search, the particles show a match to cellulose but with a low matching value. Most likely, these particles are charred cellulose. There are pronounced differences in FTIR spectra across the whole spectral range between cellulose and the particles. In particular, the peaks associated with the O-H group, such as those at 3600-3100 cm^{-1} (stretching vibration of the hydrogen bonded O-H in polysaccharides), 1630-1650 cm^{-1} (the O-H bending from the water molecules absorbed in cellulose), and 2940 and 2860 cm^{-1} (asymmetric and symmetric stretching vibrations of the C-H hydroxyl groups), are either absent or present at much lower intensities, suggesting the dehydration reactions during the cellulose → charred cellulose transformation. In addition, the peak at ~900 cm^{-1}, which is attributed to β-glycosidic linkage between glucose units, is absent, suggesting the breakage of the pyranose linkage in cellulose. The peaks associated with the pyranose, such as those at 1428 cm^{-1} and 1370 cm^{-1} (CH_2 and CH bending of pyranose ring), and 1034 cm^{-1} (C-O-C pyranose ring vibration), are preserved but with decreased intensity[4-5].

It should be noted that µ-ATR often provides the best S/N for the resulting spectrum, which lends itself to library searching. In addition, it requires little to no sample preparation, whereas other modes of analysis often involve sample preparation steps such as flattening the samples for reflectance analysis or compressing the samples into thin sections for transmission analysis.

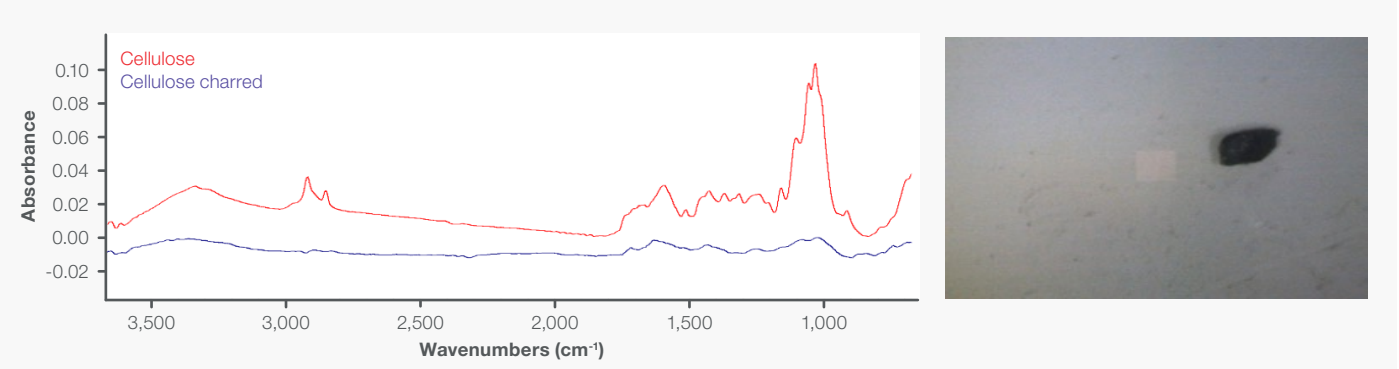

Figure 4. ATR FTIR spectrum of a black particle in the recycled PE pellets.

Analysis of the particles present in grocery bags by transmission FTIR microscopy

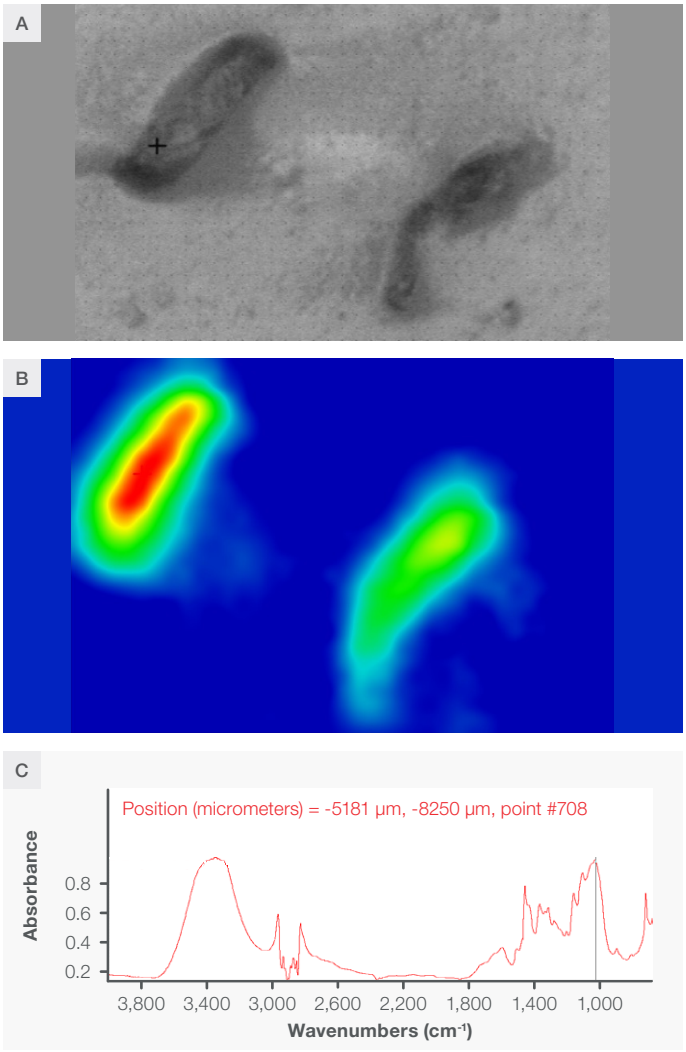

Figure 5. Transmission FTIR microscopy of grocery bag made from recycled LDPE. (A) Optical image of a piece of grocery bag showing two particles embedded in the sample matrix. (B) Chemical map of the sample constructed using cellulose spectrum as the refence. (C) FTIR spectrum of the grocery bag sample with PE spectrum subtracted.

The grocery bag was made out of recycled LDPE. A small piece was cut and analyzed in the transmission mode with no further sample preparation. Two particles were located (Figure 5A). Due to the thickness of the film, the peaks are saturated. In order to extract the spectrum of the contaminant particles, the PE peaks were subtracted from the total spectrum and the resulting spectrum is shown in Figure 5C. The ensuing search shows a match to cellulose. Correlation profiling using the cellulose spectrum results in the chemical image shown in Figure 5B.

Conclusions

In this application note, FTIR microscopy was successfully applied for the analyses of the contaminants found in recycled polymers. In all samples analyzed, cellulose, in either its native or charred form, was identified as a contaminant. The comparison between cellulose and charred cellulose provides an insight to the difference in their underlying chemistry, which can be beneficial for understanding the origins of the contaminants as well as their associated recycling processes. Additional fibrous contaminants, PET, and acrylonitrile butadiene, were identified in the recycled HDPE pellets, illustrating the chemical specificity of FTIR microscopy. Three sampling modes—reflectance, µ-ATR, and transmission—were used for the analyses, demonstrating the flexibility and versatility of FTIR microscopy to suite different sample types.

References

1. Francisco Vilaplana, Sigbritt Karlsson, Quality Concepts for the Improved Use of Recycled Polymeric Materials: A Review, *Mater. Eng.* 2008, 293, 274–297
2. Bina Bhattarai, Yukihiro Kusano, Tommy Licht Cederberg, Lisbeth Krüger Jensen, Kit Granby, Gitte Alsing Pedersen, Chemical characterization of virgin and recycled polyethylene terephthalate films used for food contact applications, *European Food Research and Technology* (2024) 250:533–545.
3. Viola Hospodarova, Eva Singovszka, Nadezda Stevulova, Characterization of Cellulosic Fibers by FTIR Spectroscopy for Their Further Implementation to Building Materials, *American Journal of Analytical Chemistry*, 2018, 9, 303-310.
4. Ivana Pastorova, Robert E. Botto, Peter W. Arisz, Jaap J. Boon, Cellulose char structure: a combined analytical Py-GC-MS, FTIR, and NMR study, *Carbohydrate Research*, 1994, 262 (1), 27-47.
5. Nicole Labbe, David Harper, Timothy Rials, Chemical Structure of Wood Charcoal by Infrared Spectroscopy and Multivariate Analysis, *Agric. Food Chem.* 2006, 54, 3492-3497.

Spectroscopy

Classification of polyethylene by Raman spectroscopy

Authors

Mohammed Ibrahim, Ph.D.,
Herman He, Ph.D.,
Thermo Fisher Scientific, USA

Keywords

DXR3 Raman microscope, polyethylene (PE), density, Raman spectroscopy, Raman microscopy, classification, discriminant analysis

Thermo Scientific™ DXR3 Raman Microscope.

Application benefits

Raman spectroscopy provides molecular level structural information, and is advantageous in classifying polyethylene (PE). Sample preparation is minimal. The method is non-destructive, and the analysis is fast (once the TQ methods are established).

Introduction

Polyethylene (PE) is one of the most common plastics in the world with annual global production of around 80 million tons.[1] Based on density, polyethylene is generally classified as high-density polyethylene (HDPE, > 0.940 g/cm^3) or low-density polyethylene (LDPE, < 0.930 g/cm^3).[2] These different density polyethylene's have vastly different physical, chemical, and mechanical properties, and hence are used in different applications. For example, HDPE is primarily used for milk jugs, detergent bottles, garbage containers, and water pipes, due to its high tensile strength; LDPE, on the other hand, has a lower tensile strength and is used mainly for plastic bags and wraps. Therefore, density is one the most important properties of polyethylene, and classifying them according to their density is essential for proper PE specification.

Bulk PEs are manufactured as pellets (resins, granules), and later converted to other forms (such as films and pipes) using extrusion or molding processes. They are also made into multilayer films for a wide range of industrial applications like food and consumer product packaging. The density of bulk PE pellets and single-layer PE films can be measured and classified with relative ease using several standard techniques: ISO 1183-1/ASTM D792 (immersion method),[3] ISO 1183-2/ASTM D1505 (density gradient method),[4] and ASTM D4883 (ultrasound method).[5] However, all these techniques require the PE in its "pure" form, which can be challenging in the case of PE in multilayer films. Extensive sample preparations (microtoming, separation of layers by dissolving in solvents) are often required[6] to isolate the PE layer before analysis, which can be labor-intensive and time-consuming.

Raman spectroscopy is sensitive to changes in the molecular structure level of PE, such as the degree of crystallinity, which is the key determining factor of PE density.[7,8] More importantly, the confocal capability of Raman microscopy allows for facile *in situ* analysis of individual PE layers in multilayer films without the need to isolate the PE layer. To our best knowledge, PE density measurement using Raman has been limited to PE pellets.7,8 In this work, we want to systematically explore the feasibility of using

confocal Raman microscopy for PE film density analysis, both qualitatively and quantitatively. We demonstrate that Raman microscopy in combination with the discriminant analysis method can be successfully applied to distinguish HDPE and LDPE in both pellet and film forms. In a subsequent application note, we will detail the quantitative determination of PE density using a confocal Raman microscope.

Experimental

Sample description

A total of 16 PE samples (10 pellets and 6 films) with known densities were used for the classification studies. All samples were used as received.

Method description

A Thermo Scientific™ DXR2 Raman Microscope was used for the collection of Raman data. For each type/class of the pellet samples, Raman spectra were collected from 3 different pellets and averaged. For each film sample, Raman spectra were collected from 3-4 locations across the surface of the sample. An averaged spectrum was then used for final analysis.

A 532 nm laser was used with a 2 mW laser power at the sample. A 10x objective and a 50 µm slit aperture were used to obtain more representative spectra from the samples. Total acquisition time for each spectrum was 30 seconds (3 second exposure x 10 exposures). Thermo Scientific™ OMNIC™ software was used for operation of the DXR2 Raman Microscope, and collection of Raman spectra; Thermo Scientific™ TQ Analyst™ software was used for chemometric analysis of the Raman data.

Results and discussion

Raman spectra

Representative Raman spectra of HDPE and LDPE samples, in both pellet and film forms, are shown in Figure 1. There are noticeable differences between HDPE and LDPE spectra, for both pellets and films. In the CH_2 bending and the CH_2 twisting region, the intensity of the CH_2 bending mode at 1416 cm^{-1} (relative to the CH_2 bending mode at 1440 cm^{-1}) is higher for HDPE than for LDPE. This observation agrees with the previous reports that the 1416 cm^{-1} and 1440 cm^{-1} peaks are indicators of crystalline and amorphous PE phases, respectively.[7-10] The higher the degree of crystallinity, the higher the density. The differences between HDPE and LDPE are also pronounced in the C-H stretching region. The intensity of the symmetric CH_2 stretching mode at 2848 cm^{-1} (relative to the asymmetric CH_2 stretching mode at 2882 cm^{-1}) appears to be higher for LDPE compared to HDPE. Since the C-H stretching (2825-2970 cm^{-1}) and the CH_2 bending regions (1398-1470 cm^{-1}) are sensitive to the density of PE, these regions were selected for subsequent discriminant analysis.

Data processing

The raw Raman spectra were processed using Norris 2nd derivative, and the resulting spectra were further processed by standard normal variate (SNV). Examples of the data processing are shown in Figure 2. Norris derivative is effective in removing background drift in Raman spectra caused by fluorescence, whereas SNV is effective in compensating such variations as sample surfaces and laser penetration depths.[11-12]

The discriminant analysis classification method with principal component analysis (PCA) algorithm[13] from the TQ Analyst software package was applied to distinguish HDPE vs. LDPE. A total of 12 samples, a mix of pellets and films, were used as the calibration standards. Four additional samples (one HDPE pellet, one HDPE film, one LDPE pellet, and one LDPE film) were selected as the validation standards (Table 1). PCA derives the principal components (PC) or the significant spectral information from the spectral variance of the calibration sample set. The number of significant PCs represents the number of independent variables affecting spectral responses, including but not limited to: concentration, impurities, opaqueness, and

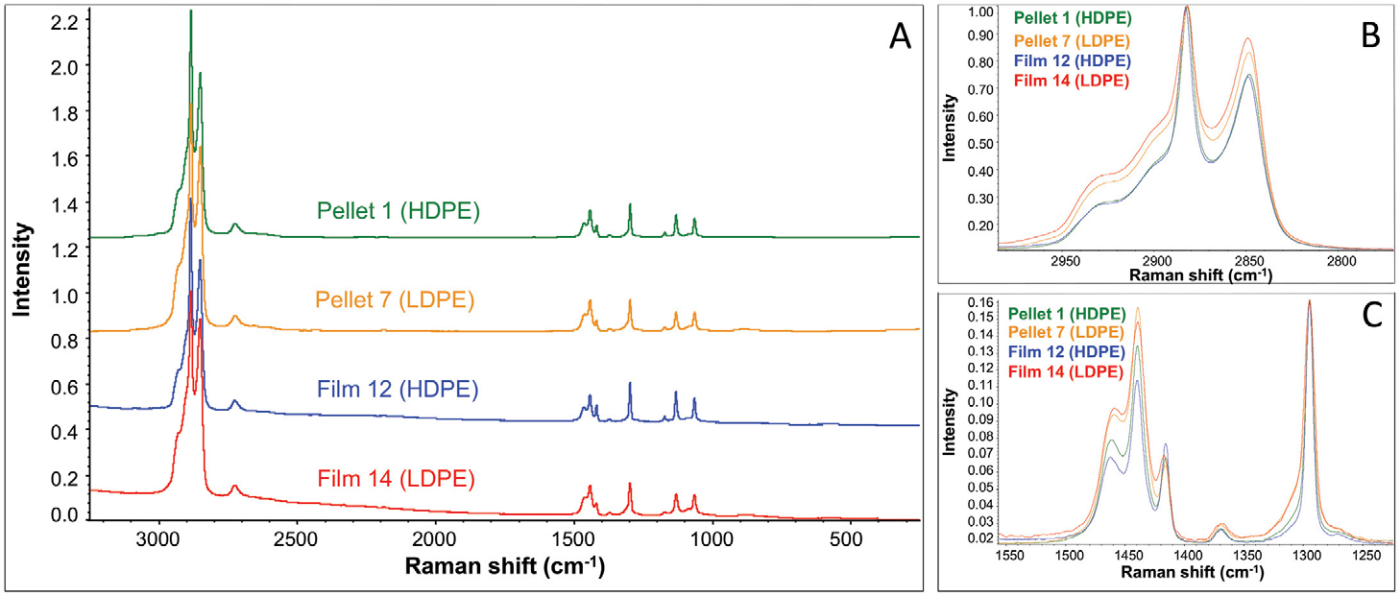

Figure 1. Representative Raman spectra of HDPE and LDPE pellets and films. (A) Full spectral range. (B) C-H stretching region. (C) CH_2 bending and CH_2 twisting region.

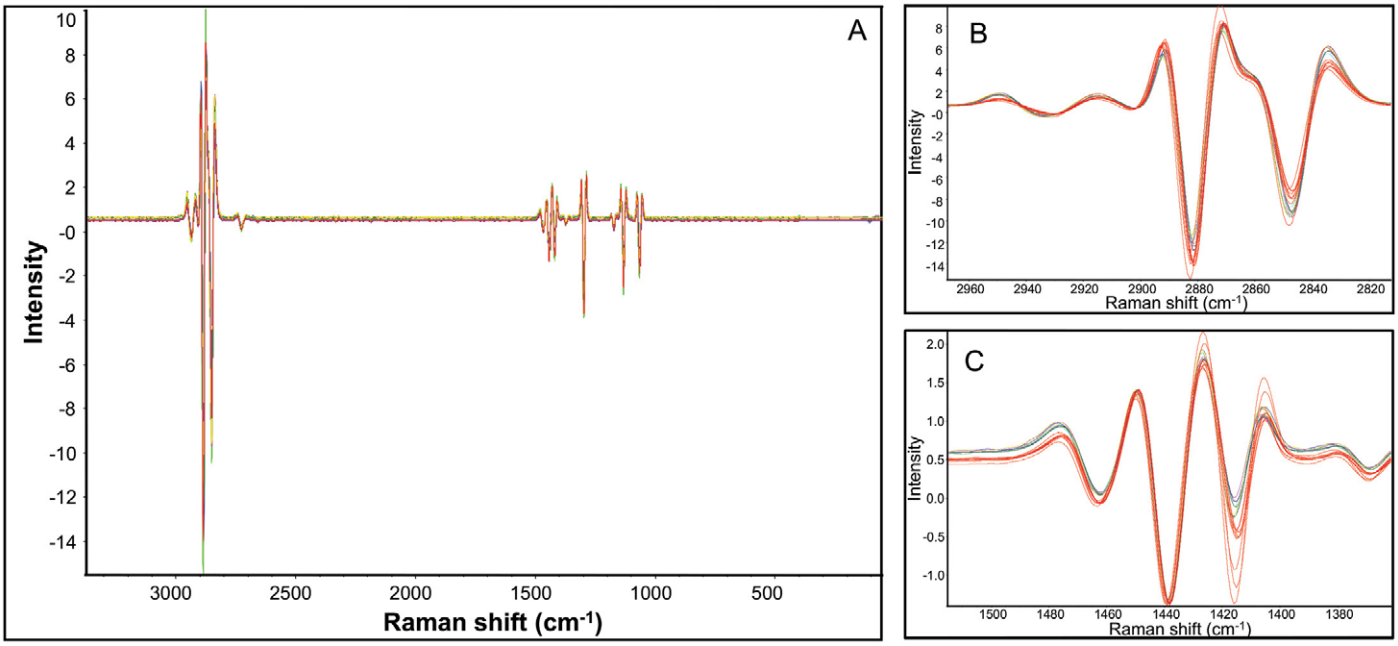

Figure 2. Norris 2nd Derivative and SNV processed sample spectra. (A) Full spectral range. (B) C-H stretching region. (C) CH_2 bending region. HDPE spectra are in red in both B and C Plots.

Classification of PE by discriminant analysis

				Calibration results		
	PE sample	Actual class	Usage	Calculated class	Distance to HDPE	Distance to LDPE
Pellets	1	HDPE	Calibration	HDPE	0.89	4.23
	2	HDPE	Calibration	HDPE	0.77	4.97
	3	HDPE	Calibration	HDPE	0.67	4.05
	4	HDPE	Validation	HDPE	1.33	3.69
	5	HDPE	Calibration	HDPE	0.68	5.14
	6	HDPE	Calibration	HDPE	0.76	4.91
	7	LDPE	Calibration	LDPE	4.01	0.99
	8	LDPE	Calibration	LDPE	5.32	0.78
	9	LDPE	Validation	LDPE	3.79	0.94
	10	LDPE	Calibration	LDPE	4.71	0.77
Films	11	HDPE	Validation	HDPE	1.23	4.79
	12	HDPE	Calibration	HDPE	1.24	4.66
	13	HDPE	Calibration	HDPE	1.30	4.93
	14	LDPE	Validation	LDPE	4.97	0.84
	15	LDPE	Calibration	LDPE	4.84	0.57
	16	LDPE	Calibration	LDPE	4.54	1.19

Table 1. PE sample class types and calibration results.

sample color. Scores of PCs depict the projected sample spectrum in the principal component domain. The PCA-based classification method then calculates the Mahalanobis (M) distance, defined by the distance between the sample and the center of each cluster in the PC domain. The sample is classified as belonging to a class if M < 3, and rejected from a class if M > 3.

The number of PCs has a direct impact on the robustness of the discriminant analysis. As shown in Table 2, the first several principal components represent the majority of the spectral variation. Five PCA factors, accounting for 99.7% of the total spectral variance, were used in this classification model.

Number of PCs	Cumulative Variance%
0	0
1	80.96
2	98.03
3	98.83
4	99.46
5	99.74

Table 2. Impact of number of PCs on variance coverage.

Figure 3 is a 3-D plot of PCA Clusters of HDPE and LDPE. The HDPE samples (red) and LDPE (blue) samples are located on the opposite ends of the cube. Notwithstanding PC1 accounting for ~81% of the total spectral variation in the data set, the separation between HDPE and LDPE is mainly in the PC2 dimension. In the current case, the PC2 dimension seems to be closely correlated to the PE density. Figure 4 shows the crossvalidation results of the 16 samples, the M distance to its own class vs. the M distance to the other class. The average M distance for each sample to its own class was about 1, but the average distance to the other class is over 4, as listed in Table 1. For both sample classes (HDPE and LDPE), there is no separation between pellets and films, suggesting the sample form (pellet vs. film) has little, if any, impact on the methodology.

The Raman spectrum of a previously unused pellet sample with known density was used to test the established discriminant method, and the result is shown in Figure 5. The sample was successfully classified as HDPE with an M value of 0.68.

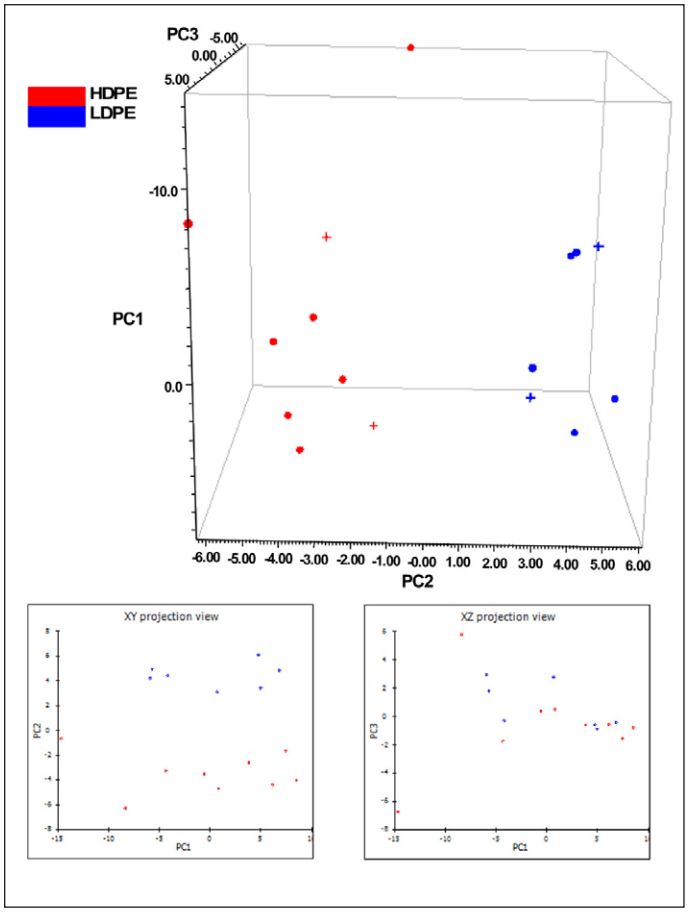

Figure 3. 3-D cluster plot of HDPE and LDPE samples. The • are the calibration samples, and the + are the validation samples.

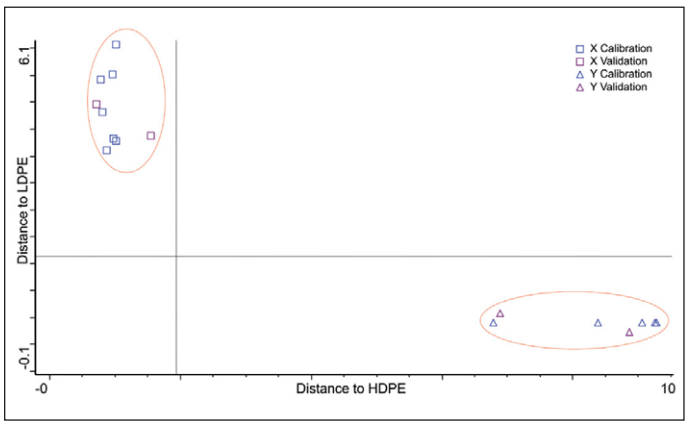

Figure 4. TQ Analyst software discriminant analysis calibration output for PEs with different densities. The two different types of PEs: HDPE and LDPE are clearly separated, and correctly classified. The calibration results are also shown in Table 1.

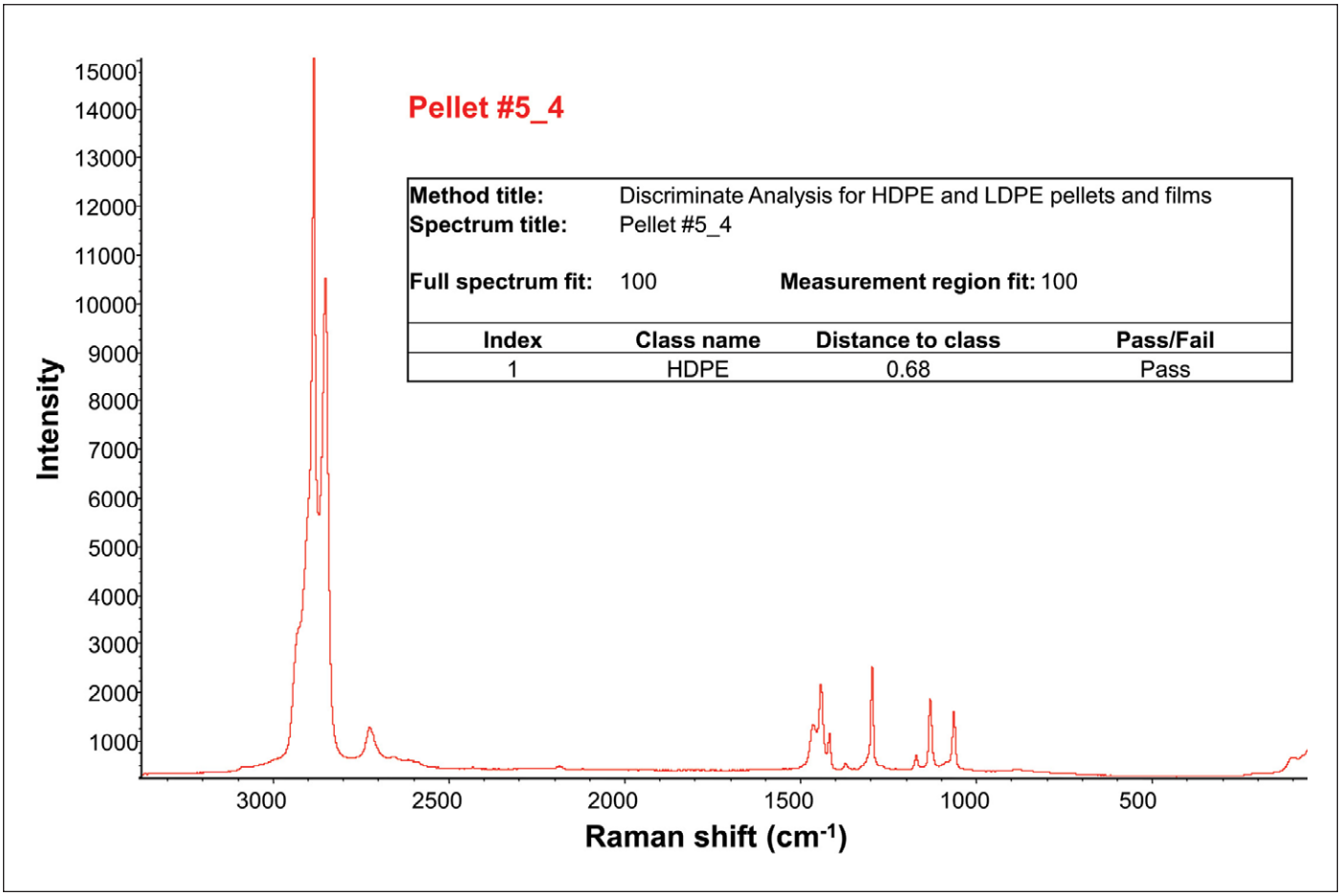

Figure 5. Classification of a PE sample by using its Raman spectrum and the discriminant method created by the TQ Analyst software.

Conclusion

In this application note, we have successfully demonstrated the use of a Thermo Scientific DXR2 Raman Microscope, in combination with the TQ Analyst software, to classify polyethylene's of different density classes in both pellet and film forms. Raman spectroscopy is nondestructive and requires minimal sample preparation. The classification method was created solely based on the Raman spectral features of LDPE and HDPE and was indifferent to the sample forms. Once the method is established, PE samples, pellets or films, can be correctly classified within minutes. Moreover, this work expands the scope of the previously reported study on PE pellets to include PE films, which broadens its applicability in the plastic/polymer industry as well as many downstream industries. The described methodology should be applicable for in situ classification of thin PE layer(s) in multilayer films.

The data were collected using an older model instrument DXR2 Raman microscope. Currently, Thermo Fisher Scientific offers an improved model, the DXR3 Raman Microscope, which offers superior speed and performance over its predecessor model.

References

1. Piringer O.G. and Baner A.L., ed. *Plastic Packaging: Interactions with Food and Pharmaceuticals*. 2nd ed. Weinheim: Wiley-VCH; 2008.
2. Polyethylene, *The Essential Chemical Industry - online*, http://www.essentialchemicalindustry.org/polymers/polyethene.html, retrieved on 9/10/2017.
3. (a) ISO 1183-1:2012, Plastics – Methods for determining the density of non-cellular plastics – Part 1: Immersion method, liquid pyknometer method and titration method; ANSI New York, NY. (b) ASTM D792-13, Standard test methods for density and specific gravity (relative density) of plastics by displacement; *ASTM International*, West Conshohocken, PA, 2013.
4. (a) ISO 1183-2:2004, Plastics – Methods for determining the density of non-cellular plastics – Part 2: Density gradient column method. (b)ASTM D1505-10, Standard test method for density of plastics by the density-gradient technique; *ASTM International*, West Conshohocken, PA, 2010.
5. ASTM D4883-08, Standard test method for density of polyethylene by the ultrasound technique; *ASTM International*, West Conshohocken, PA, 2008.
6. Mieth A., Hoekstra E., and Simoneau C. Guidance for the identification of polymers in multilayer films used in food contact materials: *User guide of selected practices to determine the nature of layers, EUR 27816 EN*, 2016; doi: 10.2788/10593.
7. Strobl G.R. and Hagedorn W. Raman spectroscopic method for determining the crystallinity of polyethylene, *J. Polym. Sci. B Polym. Phys.*, 1978, 16, 1181-1193.
8. Sato H., Shimoyama M., Kamiya T., Amari T., Sasic S., Ninomiya T., Siesler H.W., and Ozaki Y. Raman spectra of high-density, low-density, and linear low-density polyethylene pellets and prediction of their physical properties by multivariate data analysis, *J. Appl. Polym. Sci.*, 2002, 86, 443–448.
9. Migler K.B., Kotula A.P., Hight Walker A.R. Trans-rich structures in early stage crystallization of polyethylene, *Macromolecules*, 2015, 48, 4555–4561.
10. Kida T., Hiejima Y., and Nitta K-H. Raman spectroscopic study of high-density polyethylene during tensile deformation, *Int. J. Exp. Spectroscopic Tech.*, 2016, 1:001.
11. Simone, E., Saleemi A.N., and Nagy Z.K. Application of quantitative Raman spectroscopy for the monitoring of polymorphic transformation in crystallization processes using a good calibration practice procedure, *Chem. Eng. Res. Des*. 2014, 92, 594–611.
12. Huang J., Romero-Torres S., and Moshgbar M. Practical considerations in data pre-treatment for NIR and Raman spectroscopy, *Am. Pharm*. Rev. 2010, 13 (6).
13. Thermo Scientific Product Overview. *TQ Analyst Software Chemometric Algorithms*, 2009.

Visit the Raman academy that has many Raman video lessons.

Learn more at **thermofisher.com/microplastics**

Combined FTIR and Raman microspectroscopy analysis of laminates

Multilayer polymer laminate packaging materials are carefully engineered composite materials in which different polymer layers are selected to provide specific physical and chemical characteristics. This way, it is possible to customize properties such as mechanical strength and flexibility and to add barriers to environmental factors such as gases, moisture, and light. There is considerable variation in the thickness of the different polymer layers, ranging from a micron or less to more than 100 microns thick.

Confirming the identity of the various layers, as well as the thickness, is important for quality assurance and failure analysis, as well as for the reverse engineering of unknown multilayer polymer materials. Both Fourier transform infrared (FTIR) and Raman spectroscopy can be used to identify and distinguish among a wide range of different polymeric materials. When these techniques are coupled with a microscope, they are uniquely suited for the analysis of the individual layers in such multilayer materials.

FTIR and Raman microspectroscopy are often regarded as complementary techniques. Both are vibrational spectroscopy techniques that provide information about chemical identity and molecular structure, but there are some distinct differences. FTIR selectivity is based on dipole moments, so it tends to be better at emphasizing the different functional groups found in polymers, such as carbonyls, esters, amides, and hydroxyl constituents. There also tends to be a greater number of FTIR libraries available, which is an advantage in the identification of unknown materials. Raman selectivity is based on polarizability and tends to emphasize polymer backbones as well as delocalized bonding such as aromatic structures. Raman spectroscopy provides easier access to lower wavenumber parts of the vibrational spectrum, making it is easier to observe molecules with heavier atoms, such as inorganic pigments. Because visible Raman spectroscopy utilizes visible lasers, it can achieve better spatial resolution than FTIR microspectroscopy. While both techniques have advantages and disadvantages, they are both very effective for the analysis of individual layers in multilayered polymer packaging materials.

This technical note will compare the results of the analysis of a cross-section of a multilayer polymer laminate using both FTIR and Raman microspectroscopy. It was necessary to obtain a thin cross-section for FTIR transmission analysis. While this was not necessary for the Raman analysis, the same cross-section was used for both analyses to avoid any potential variations that might arise from different sample preparation methods.

Experimental

The cross-section of the multilayer laminate was prepared by sandwiching the polymer film between two rigid layers of polytetrafluoroethylene (PTFE). This assembly was clamped in a holder, and thin cross-sections were obtained using a Thermo Scientific™ Shandon Finesse™ E+ Microtome. Cross-sections of the multilayer polymer film were easily separated from the PTFE and were positioned flat on a barium fluoride window for analysis. The FTIR microscopy analysis was carried out in transmission mode using a Thermo Scientific™ Nicolet™ RaptIR™ FTIR Microscope, and the Raman analysis was done using a Thermo Scientific™ DXR3xi Raman Imaging Microscope.

DXR3xi Raman Imaging Microscope and Nicolet RaptIR FTIR Microscope.

FTIR analysis results

The Nicolet RaptIR FTIR Microscope makes finding the sample on the window simple by first quickly collecting a high-quality visual mosaic of the entire window using a 4X visual objective and then automatically switching to the 15X infrared objective. The initial mosaic provides a visual guide to allow the user to find samples and areas of interest, and the 15X objective allows for more detailed visual mosaics, as well as infrared analysis. Figure 1 illustrates this workflow, showing both the large 4X visual mosaic as well as the higher magnification visual mosaic. The defined area shown in Figure 1 is the portion of the cross-section that was analyzed. The aperture was 5 microns in the direction perpendicular to the polymer layers, and spectra were collected across the cross-section using 2-micron steps.

Figure 2 shows an FTIR image based on a multivariate curve resolution (MCR) analysis. This analysis compares each spectrum to all the other spectra in the image and groups similar spectra together as components. The various components are assigned a color to generate the image. In this case, there are five different components (blue, green, light blue, yellow, and red) and six different layers. The advantage of the MCR analysis is that no prior knowledge of specific spectral features is required for the analysis.

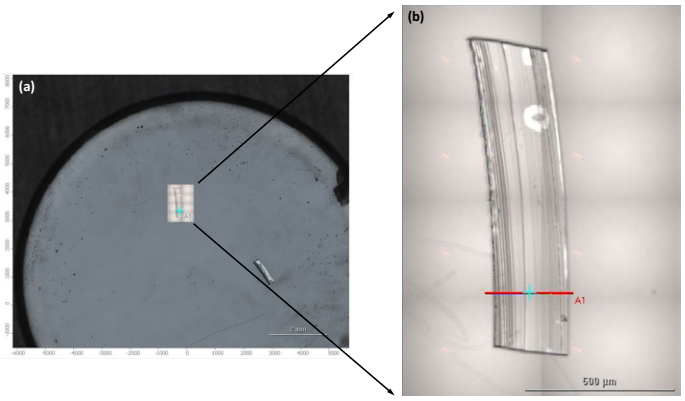

Figure 1: (a) Initial visual mosaic image collected with a 4X visual objective showing essentially the entire barium fluoride window. This view is used to locate the cross-section on the window. (b) Second visual mosaic of the cross-section collected with the 15X infrared objective. Area A1 indicates the portion of the cross-section that was analyzed.

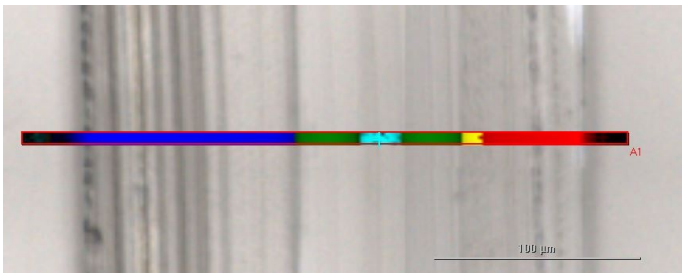

Figure 2: MCR FTIR image of the cross-section of the multilayer polymer film. Each color represents a different polymer material; there are five different polymer materials and six layers.

These results can be used as a starting point for utilization of some of the other profile choices that might better define the various layers. The FTIR images in Figure 3 are based on correlation profiles using the spectra shown as the reference spectra. Searching the spectra against libraries can help to identify the various layers. Layer 5 was identified as poly(propylene-ethylene) by comparison of the spectrum to spectra from layers 1 and 6. The thicknesses of the various layers were measured using the ruler tool provided in the software. In this way, it was possible to not only identify the various layers in this multi-layer polymer film but also to determine the thickness of each layer.

Raman analysis results

The same laminate sample was analyzed using a DXR3xi Raman Imaging Microscope. Figure 4 shows the visual mosaic image obtained using a 50X objective on the Raman microscope. The defined area indicates the portion of the cross-section that was analyzed. The MCR image generated from the Raman spectra is very similar to what was seen in the FTIR analysis, in that there are five components and six layers.

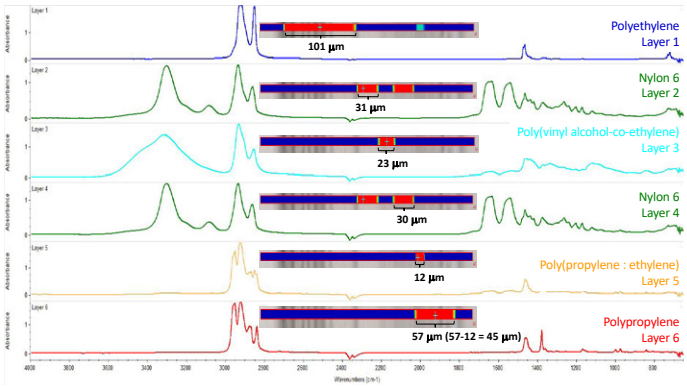

Figure 3: Representative FTIR spectra from each of the polymer layers along with associated correlation FTIR images that show the locations of the different types of polymeric materials. The materials were identified by spectral searching against commercial libraries, and the thicknesses of the layers were determined using the ruler option in the software.

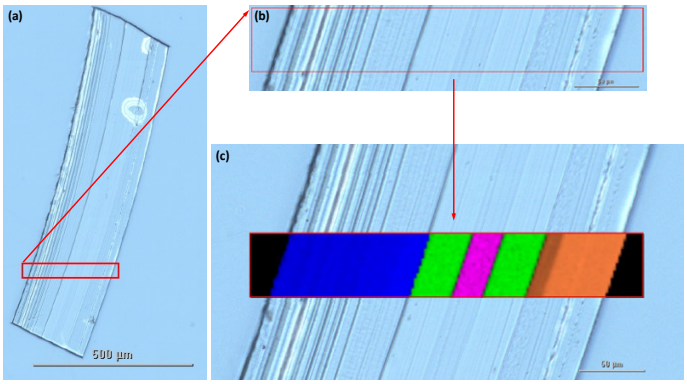

Figure 4: (a) Visible mosaic of the cross-section collected using a 50X objective on the Raman microscope. (b) Area on the cross-section selected for Raman analysis. (c) MCR Raman image showing five different polymer materials and six layers.

Each layer of the sample was defined using correlation profiles, and the results of those profiles are shown in Figure 5. It was possible to identify the various layers in the laminate by searching against Raman spectral libraries, but the Raman spectra lack the strong spectral features associated with the polar functional groups that were so readily apparent with the FTIR spectra. The N-H peaks in the nylon spectra are visible, but their appearance is much weaker in the Raman spectra compared to the FTIR spectra. Identification is even more difficult with the poly(vinyl alcohol-ethylene) layer because the O-H peak is not apparent in the Raman spectra.

It was still possible to get a library match for this spectrum, but the match was not nearly as definitive as it was with the FTIR spectrum. Conversely, the identification of the polyethylene in the poly(propylene-ethylene) layer was more readily apparent from the Raman spectra because of the presence of the 1295 cm^{-1} peak that is associated with polyethylene and that does not overlap with any polypropylene peaks. The polyethylene and polypropylene peaks in the FTIR spectra overlap quite a bit, so the differences are more subtle in these spectra.

The thicknesses of the layers were measured using the ruler tool in the software of the Raman microscope, and the thicknesses of the layers were very consistent with the values determined in the FTIR analysis. While the Raman analysis provided higher resolution, that did not really affect the determination of the layer thicknesses.

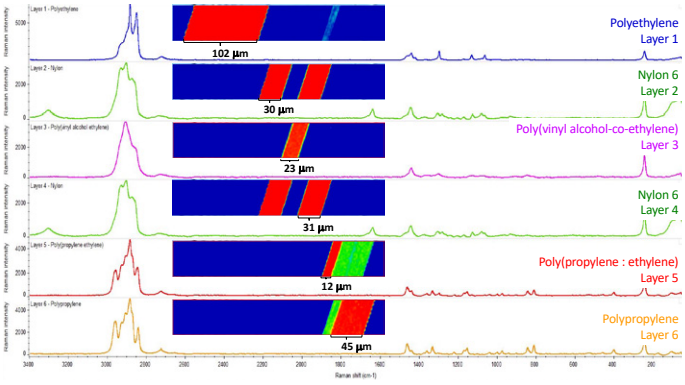

Figure 5: Representative Raman spectra from each of the six layers and the corresponding Raman correlation images showing the location of each type of polymer material. The polymer layers were identified by spectral searching against commercial libraries, and the thicknesses of the layers were determined using the ruler tool in the software.

Conclusions

FTIR and Raman microspectroscopy provided comparable results for the analysis of a multilayer polymer film. The collection times for the two data sets were similar. The step size for the FTIR mapping and the image pixel size for the Raman imaging were both 2 microns, and, clearly, any spatial resolution differences were not a factor in the analysis of this sample.

While the FTIR spectra had a slightly better signal-to-noise ratio, both the FTIR and Raman spectra were good quality and allowed for layer identification as well as layer thickness determinations. The differences in the selection rules for FTIR and Raman means that there are variations in peak intensities associated with molecular functionalities. This means that each technique highlights distinct aspects of the various polymers in the laminate. For instance, the poly(vinyl alcohol-ethylene) layer was more readily identified with the FTIR data, but the presence of the small amount of polyethylene in the poly(propylene-ethylene) layer was more apparent in the Raman data. The same cross-section was used for each of these analyses, but the Raman analysis is not a transmission technique, so it is not necessary to prepare a thin cross-section for use with the Raman microscope. This means that sample preparation for Raman analysis can be simpler and save time and effort.

There are other considerations such as fluorescence, resolution of ultra-thin layers, and the analysis of pigments that might drive the choice in one direction or another Clearly, both the Nicolet RaptIR FTIR Microscope and the DXR3xi Raman Imaging Microscope are excellent choices for the analysis of multilayer laminates.

Time-based FT-IR analysis of curing of polyurethanes

Authors

Stefano Radice, Solvay Solexis, Milan, Italy

Mike Bradley, Ph.D.,
Thermo Fisher Scientific, Madison, WI, USA

Keywords

- Adhesives
- Curing
- OMNIC Software
- Sealants
- Series Software
- Urethanes

Introduction

The construction and automotive industries make use of a huge number of vendors, supplying anything from raw materials to complete assemblies. Among the critical components for both industries are adhesives and sealants. Each application requires specific characteristics, including curing conditions (temperature, moisture and speed of cure) and long term material properties, such as flexibility, UV resistance and bond strength.

The curing and working properties of adhesives generally result from polymerization reactions, which form a lattice of chemical bonds. Basic chemical kinetics identifies four steps in these polymerizations – initiation, propagation, termination and branching. The relative rates of these determine the properties of the final polymer. For instance, the termination step can control overall polymer chain length, branching impacts the cross-linking, and propagation rate determines curing times.

The initiation step is critical. Early initiation may result in ruined product, while sluggish initiation can lead to poor or slow curing. The initiation can be stimulated chemically, as in most two-part epoxies (the hardener stimulates a reaction in the resin), via UV-irradiation (many modern dental sealants) or using temperature. Storage needs require that the initiation reaction be halted until the proper moment. Urethanes provide an excellent example, where the initiation step can be blocked until heat is applied. Failing to do this can result in railroad cars filled with solid, useless, product.

Figure 1. Examples of items produced from polyurethanes. Photo of parts provided by Plastics International.

The polyurethane reaction starts with a diisocyanate (or a poly-isocyanate) reacting with a comonomer like an alcohol (frequently a diol):

$$R\text{-}O\text{-}H + O{=}C{=}N\text{-}R' \rightarrow R\text{-}O\text{-}C(=O)\text{-}NH\text{-}R'$$

Equation 1.

Thiols and amines can also be used (instead of the alcohol) – it is the reactivity of the acidic hydrogen which drives the reaction. This reaction can be very rapid, even at room temperature, so the liquid mixture rapidly becomes a solid. This rapidity can be used to produce unique products. For instance, during manufacturing, a little water can be added to the reaction mixture. The water reacts with the diisocyanate to produce a diamine and CO_2. The CO_2 forms bubbles in the reaction mixture which are trapped within the rapidly forming polymer matrix, yielding polyurethane foam.

Shipping and storage of the liquid urethanes requires preventing the reaction (1) from occurring. This can be done by reacting the isocyanate with a “blocker”:

$$R''\text{-}NHC(=O)\text{-}B \rightarrow R''\text{-}N{=}C{=}O + BH$$

Equation 2.

where BH is the blocking agent. The blocking group can be eliminated at elevated temperatures, yielding the reactive isocyanate and initiating the cross-linking reaction. Different blocking agents will eliminate at different temperatures, so research into the best adapted blockers (least toxic, lowest deblocking temperature, etc.) is underway.

A key part of investigating blocking agents requires studying the temperature dependence of the initiation and the time-evolution of the reaction mixture. Infrared is ideally suited to this, as the spectrum gives specific information regarding the progressing reaction. In the study highlighted here, FT-IR was able to elucidate both the progression and the mechanism for a crosslinking reaction.

Experimental

A Thermo Scientific™ Nicolet™ FT-IR spectrometer was used to collect infrared spectra at 15 second intervals, using 8 scans at 2 cm^{-1} resolution. The spectrometer was equipped with a KBr beam splitter and and DTGS detector. Our Thermo Scientific™ OMNIC™ spectroscopy software with the time-based Series™ software module was used to collect, process and present the data.

A perfluoropolyether diol (PFPE, Solvay Solexis) was mixed with ketoxime blocked isophorone diisocyanate (K-IPDI or IPDI once unblocked, Hüls-Degussa) in butyl acetate. This mixture was placed into a variable temperature cell, which was purged with dry air to remove volatiles during the reaction. The data reported here were obtained with an operating temperature of 150 °C.

Discussion

Table 1 gives the assignments for some of the observed infrared peaks.

Peak location (cm^{-1})	Chemical structure	Motion
3420-3200	N-H	Stretching
3000-2800	CH_2 and CH_3	Stretching
2260	NCO	Stretching
1740	C=O	Non-bonded urethane stretching
1690	C=O	Associated urethane and isocyanurate ring stretch
1510	H-N-C=O Amide II	Combined motion

Table 1. Assignment of major peaks, from references 1 and 2.

Figure 2 shows individual spectra taken at a series of time slices, and Figure 3 shows a large region of the dataset in the 3-D presentation of Series software. The 2260 cm^{-1} NCO peak can be seen to grow after initiation (as the blocker is removed), then disappear as the polymerization proceeds. The N-H blocking agent peak at 3420 cm^{-1} disappears rapidly. This is more clearly shown in the functional group time profiles in Figure 4.

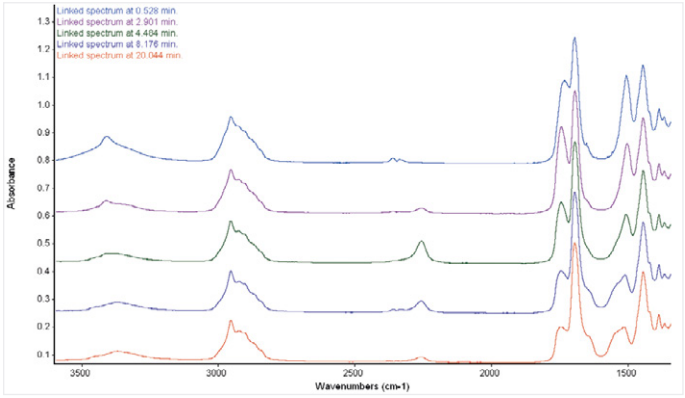

Figure 2. Time slices of spectra for the blocked urethane.

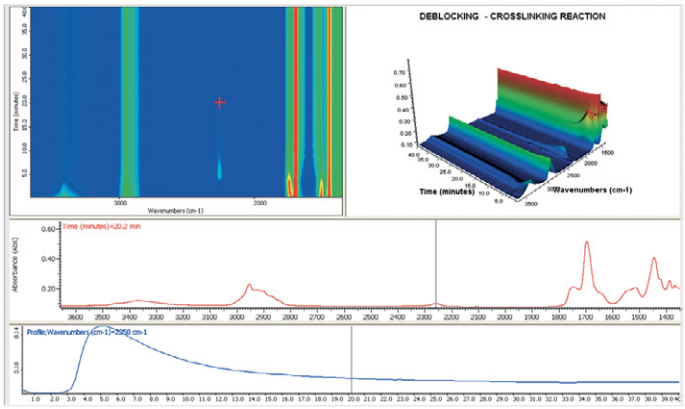

Figure 3. 3-D presentation of entire Series data set for the curing of the blocked urethane.

The intriguing aspect of this analysis is the insight into the reaction mechanism obtained from the profiles. Reactions (1) and (2) can occur sequentially (elimination (2) followed by addition(1)) or in a concerted manner (addition of the alcohol to the blocked isocyanate followed by elimination of the blocker). In the first case, the isocyanate intermediate would form immediately after the removal of the blocker, in the latter, the isocyanate would not form, or would form only later as thermally induced reversions of the urethane to the isocyanate. The data shown in Figures 3 and 4 supports the latter mechanism. The isocyanate does not form immediately upon unblocking, but shows a time delay consistent with thermal reversion of the urethane.

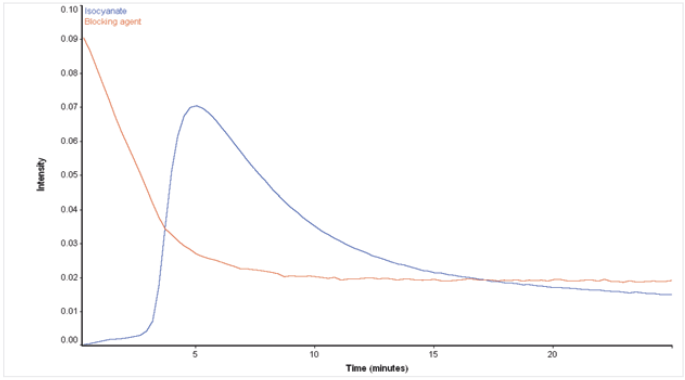

Figure 4. Time profiles of the intensity of the NCO and NH (blocking agent) during reaction.

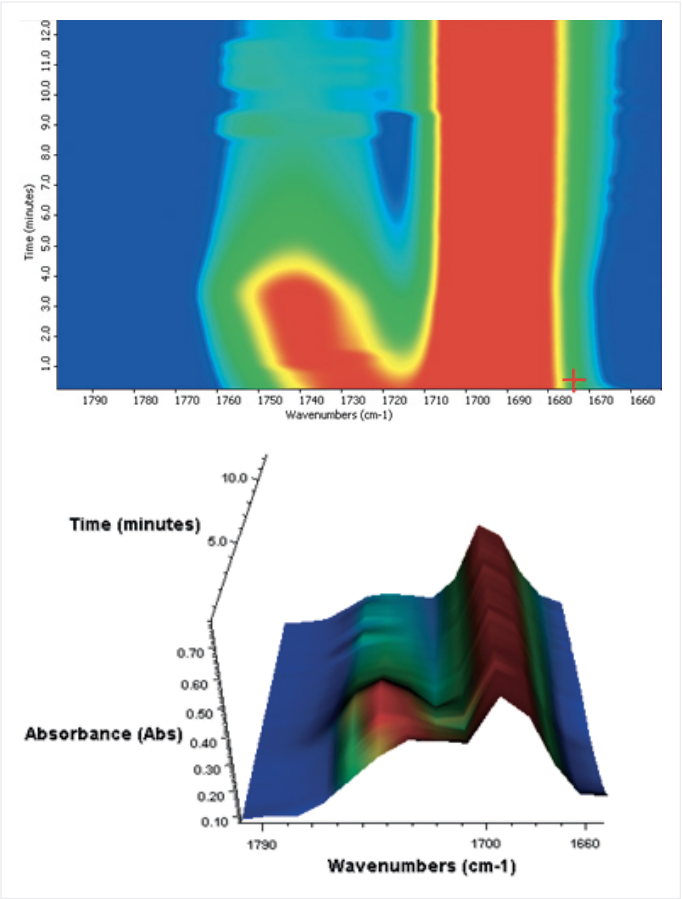

Figure 5. Contour and 3-D plot showing the shifting of the C=O peak as discussed in text.

Additional support for this mechanism is provided by the shift of the C=O band from 1734 to 1744 cm^{-1}. This is seen clearly in the contour and 3-D plots of a narrow region shown in Figure 5. The shift in the carbonyl peak is typical for urethanes close to fluorine.

Conclusion

The study of polymerization reactions requires the ability to take spectra against a time base under a wide range of conditions. The OMNIC Series software allows complete control over the experimental conditions, data collection parameters and starting trigger point. Further, the presentation capabilities provide excellent insights into subtle changes within the spectra.

Acknowledgement

The data was kindly provided by Solvay Solexis (http://www.solvaysolexis.com/). The analysis is largely based upon the discussion in the first reference.

References

1. Radice, S.; Turri, S.; Scicchitano M. Applied Spectroscopy 58(5), 2004, pp.535–542.
2. Turri, S.; Scicchitano, M; Marchetti, M.; Sanguineti, A.; Radice, S. in Fluoropolymers 2: Properties, (New York, Kluwer, 1999), p. 145.

Monitoring the UV cure process of a polymer based ink by FT-IR

Keywords

- FT-IR/polymers
- Inks
- Macros\Basic
- Paints & Pigments/ HATR/Quant
- Solid coatings

Introduction

The degree of cure of a polymer-based ink applied to a Mylar film is readily determined by FT-IR. The ink is screened onto the Mylar film and then exposed to UV light to cure the ink. The determination of percent cure is an important quality control (QC) tool and may also be used to optimize the product manufacturing process.

Experimental

Spectra were collected using a Thermo Scientific™ Nicolet™ FT-IR spectrometer and a Smart Multi-Bounce horizontal ATR accessory with a zinc selenide crystal. The ATR sampling technique was chosen for this analysis to enhance the spectral response of the inked surface and to minimize the response of the bulk Mylar film base. The inked side of the Mylar film sample was simply pressed onto the surface of the ZnSe crystal of the ATR accessory. No sample preparation was required. Spectra were collected at 4 cm^{-1} with 32 sample scans (40 second sample collection time).

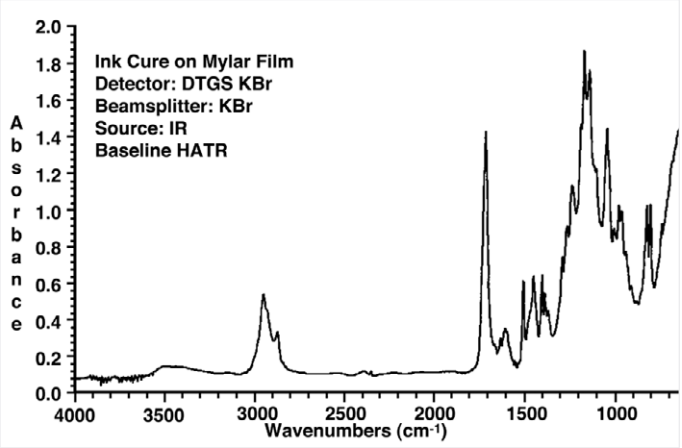

Figure 1.

Results

Figure 1 shows the spectrum of the sample prior to UV irradiation.

For this particular ink, the peak of interest is at 810 cm^{-1} and is related to free acrylate monomer. As the ink cures, there will be less of this free monomer, so the intensity of this peak will decrease. In order to quantify the degree of polymerization, an internal standard peak is needed. For this ink, the peak at 830 cm^{-1} is unrelated to the cure chemistry and remains unchanged. It is a simple exercise to monitor the ratio of these two peak heights in order to determine the amount of polymerization that has occurred during the cure process.

Figure 2 shows six spectra from the polymerization process with percent of cure ranging from 0 to 87%. Note that for these six spectra autoscaled on the 830 cm^{-1} absorbance, the band at 810 cm^{-1} varies in intensity. Where the peak heights of the 830 cm^{-1} and 810 cm^{-1} bands are nearly identical, the ink is uncured. Where the peak height of the 810 cm^{-1} band is lowest with respect to the 830 cm^{-1} absorbance the ink is 87% cured.

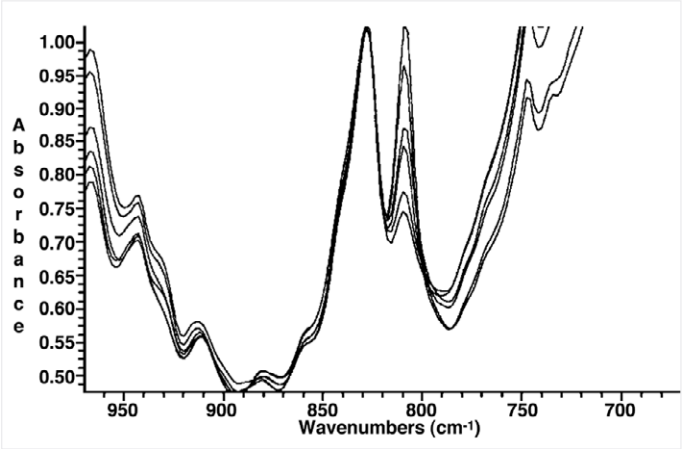

Figure 2.

Figure 3 shows a simple macro, written using Thermo Scientific™ OMNIC™ Macros\Basic™ software, that computes the ratioed peak height of 810 cm^{-1}/830 cm^{-1} for each sample spectrum using a base-line correction point at 895 cm^{-1}.

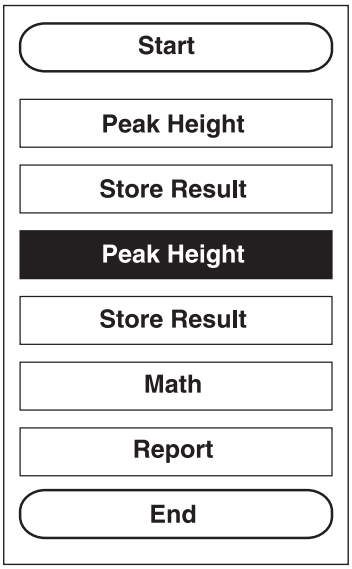

Figure 3.

The plot in Figure 4 shows a linear relationship between percent cure and the ratioed peak area. The physical properties of the cured ink are then related to the percent cure to determine the optimal manufacturing process for the UV cured ink based upon the QC determination of the spectral band ratios.

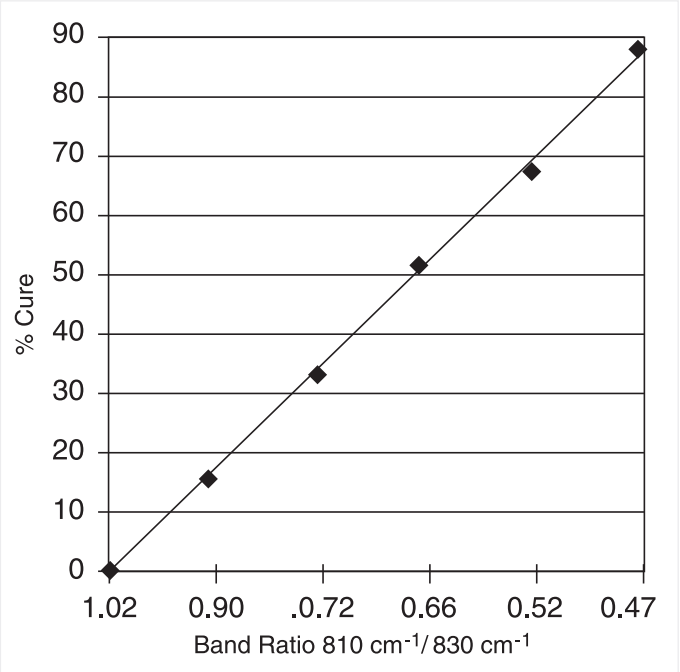

Figure 4.

Conclusion

The use of FT-IR with ATR sampling provides a fast and easy determination of the quality and state of UV curable polymerization in inks.

Sampling considerations for the measurement of a UV stabilizer in polymer pellets using FT-NIR spectroscopy

Keywords
Antaris, additives, FT-NIR, polymer, polystyrene, sample cup, spinner

Abstract

For heterogeneous samples such as polymer pellets, it is critical to obtain a measurement that is representative of the bulk sample rather than a small fraction of the material. This is often a significant challenge when using traditional near-infrared spectroscopy sampling methods. Accessories such as the Sample Cup Spinner allow a greater amount of material to be analyzed in an automated device. In this study, two diffuse reflectance-sampling methods were compared to determine the most efficient and accurate method for sampling polystyrene pellets. A single calibration model was developed to determine the concentration of an ultraviolet (UV) stabilizer additive in polystyrene pellets. Using the two sampling methods, the concentrations of four unknown samples were determined using the single model. The results demonstrate that the Sample Cup Spinner accessory provides the optimum performance with the shortest analysis time.

Introduction

With the high production rates in the polymer industry, it is essential that a quick, accurate, and easy-to-use analytical technique is available to monitor the quality of the material produced. Traditional methods, such as titration or extraction followed by GC, require sample preparation by a trained technician and often deliver results to the production personnel after a significant time lapse. This time lag between sampling and the completion of the analysis can produce out-of-specification material, resulting in manufacturing inefficiency, high scrap levels, and the need to rework product that does not meet quality standards.

Figure 1. Sample Cup Spinner for the Thermo Scientific Antaris™ FT-NIR analyzer.

Fourier transform near-infrared (FT-NIR) is an ideal tool for at-line or near-line quality control analysis of polymer pellets. It offers several advantages over traditional quality control techniques, including:

- Availability of answers in minutes allowing faster feedback to the production personnel and improvement of process efficiency
- Ability to perform analyses at-line
- No sample preparation
- Elimination of the need for purchase and disposal of hazardous reagents
- Improved operator-to-operator reproducibility
- Reduced cost of quality control testing
- Non-destructive testing making the samples available for analysis by other techniques

For heterogeneous materials such as polymer pellets, a small sample may not be representative of the bulk material. Each pellet or group of pellets may have a slightly different composition than the next. For this reason, a representative sampling method is needed. This is often achieved by the use of a cup with a quartz window. The sample cup provides a way to analyze greater amounts of material without having to empty the first sample and replace it with a new sample from the same batch. Once the sample is placed in the cup, it can be analyzed by two methods.

1. Using the Sample Cup Spinner accessory (Figure 1), the sample can be rotated, constantly exposing new sample to the incident beam during data collection. A single spectrum is obtained that is representative of the material in the cup. The Sample Cup Spinner allows the largest volume of material to be analyzed in a single measurement..

Experimental

A set of 17 polystyrene pellet samples were obtained from a proprietary source. The concentration of a UV-stabilizing additive ranged from 42% to 58% by weight. The pellet shapes and sizes varied slightly from sample to sample. The samples were placed into the open powder sampling cup, which has a 47.8 mm quartz window, and analyzed by diffuse reflectance using the Integrating Sphere Module of the Thermo Scientific™ Antaris™ FT-NIR analyzer (Figure 2).

Figure 2. Antaris FT-NIR Solid Sampling system with Sample Cup Spinner.

The analyzer's Integrating Sphere Module provides a highly efficient method for collecting diffuse reflectance data for solid samples such as polymer pellets. A background was collected for each sample using the internal gold reference of the integrating sphere. The internal reference allows the background to be collected even if the sample cup is in place. Using Thermo Scientific™ RESULT™ data collection software, all spectra were acquired at 8 cm^{-1} resolution and 16 scans with a collection time of less than 10 seconds. Spectra used to develop the method were obtained using the Sample Cup Spinner accessory. The Sample Cup Spinner was adjusted so that the largest amount of sample possible passed through the NIR beam in one complete revolution. Thirteen of the samples were used to develop the FT-NIR model and four samples were used to validate the performance of the model using the two sampling methods.

Once the model was developed, the validation samples were analyzed and the concentration of the additive was determined 30 times each using the Sample Cup Spinner and the manual single point measurement technique. To accomplish the manual single point analysis, the sample was manually rotated approximately 40 degrees between each successive measurement.

The Thermo Scientific™ TQ Analyst™ quantitative analysis software was used for all chemometric modeling. A cross-validation using a leave-one-out protocol was used to confirm the results obtained for the calibration.

Results and discussion

One spectrum was collected for each of the samples in the calibration set (13 samples total) using the Sample Cup Spinner accessory (Figure 3).

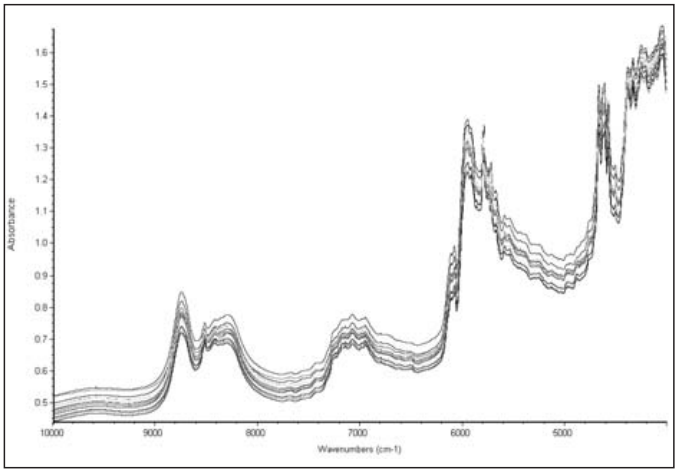

Figure 3. Calibration spectra obtained using the Sample Cup Spinner.

The total analysis time for each sample was about 15 seconds. The second derivative spectra of the calibration samples were used to develop the chemometric model (Figure 4).

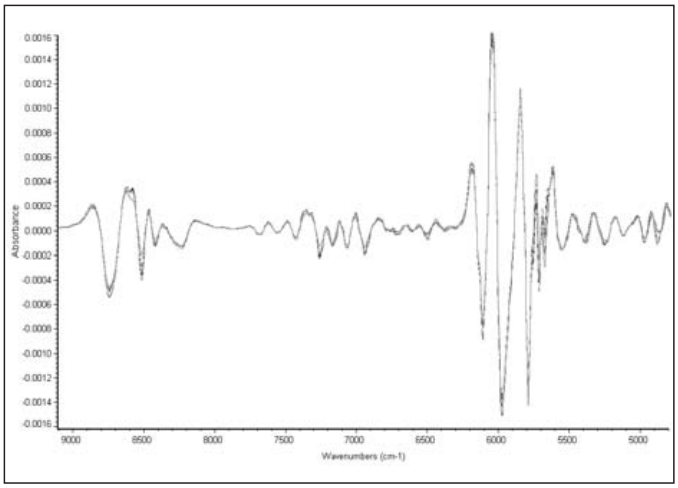

Figure 4. Second derivative spectra.

A Norris second derivative (5 segment, 0 gap) was used to pre-treat the data. A two-term Stepwise Multiple Linear Regression (SMLR) model was constructed. Using data points of 7332 cm^{-1} and 5091 cm^{-1}, a correlation coefficient of 0.9995 and RMSEC of 0.147 weight % were obtained (Figure 5). The first data point (7332 cm^{-1}) of the SMLR calibration is in the first overtone region and the second point at 5091 cm^{-1} is in the combination band region. A cross-validation using the leave-one-out protocol gave an RMSECV of 0.179 weight %.

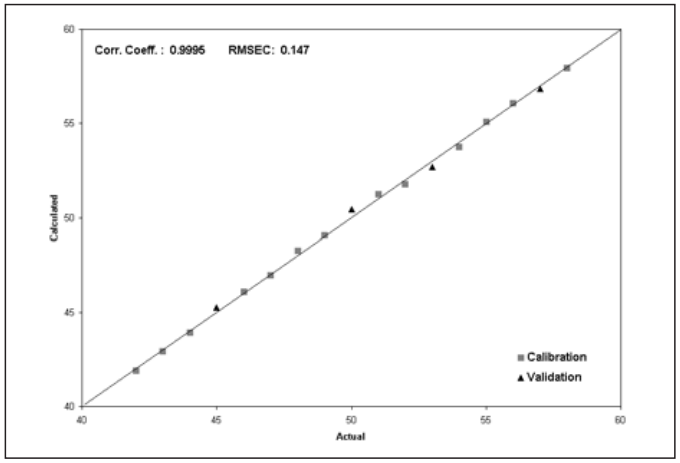

Figure 5. Calibration results using the Sample Cup Spinner.

The additive concentration in the validation samples was determined using the SMLR model. The RMSEP (Root Mean Square Error of Prediction) was 0.302 weight % for the samples analyzed using the Sample Cup Spinner. The results obtained using the Sample Cup Spinner and the manual single point measurement techniques were compared. The spectra obtained using the Sample Cup Spinner and the single point measurements are shown in Figures 6 and 7, respectively. Upon visual inspection, the spectra collected using the Sample Cup Spinner are more reproducible than those collected using the single point sampling method. The variability seen with the single point measurement method is expected because each spectrum represents only a fraction of the sample and does not account for the heterogeneity of the material. The Sample Cup Spinner continuously rotates multiple areas of the cup through the NIR beam, therefore the single spectrum that is obtained better represents the bulk of the material.

Comparison of the standard deviation of the predicted values obtained using the Sample Cup Spinner and the single point manual measurements clearly demonstrates that the Sample Cup Spinner is more reproducible and more accurately predicts the additive concentration in the validation sample (Table 1). The standard deviation of the results obtained using the single point measurement technique is two times more than that obtained using the Sample Cup Spinner. The variability in the results between the two sampling techniques for the 30 measurements is presented graphically in Figure 8.

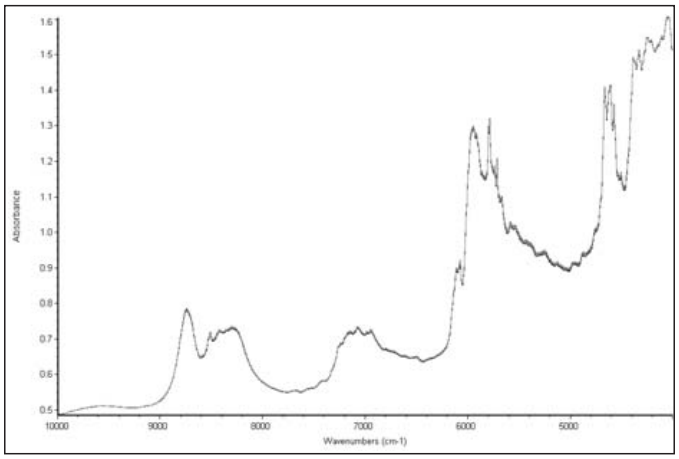

Figure 6. Spectra of unknown sample obtained using Sample Cup Spinner.

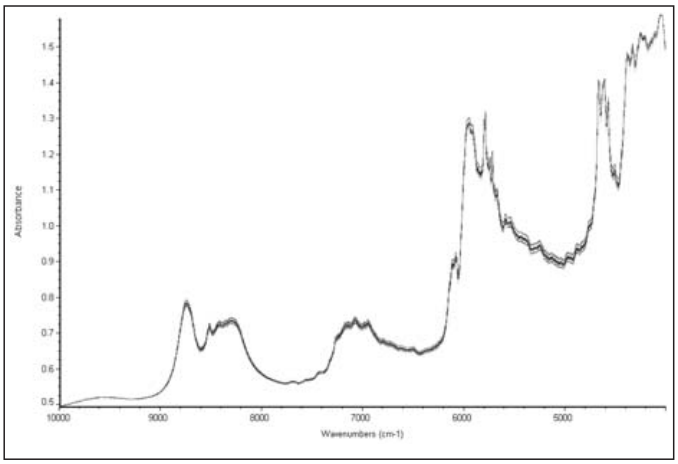

Figure 7. Spectra of unknown sample obtained using single point measurement method.

	Expected value	Sample cup spinner	Single point measurement
Validation sample 1	57	56.84	55.78
Validation sample 2	53	52.69	51.97
Validation sample 3	45	45.26	44.52
Validation sample 4	50	49.33	49.08
Standard deviation – validation sample 4		0.29	0.62
% Relative standard deviation – validation sample 4		0.29	1.27
Range – validation sample 4		1.18	2.44

Table 1. Prediction results for additive concentration (weight %).

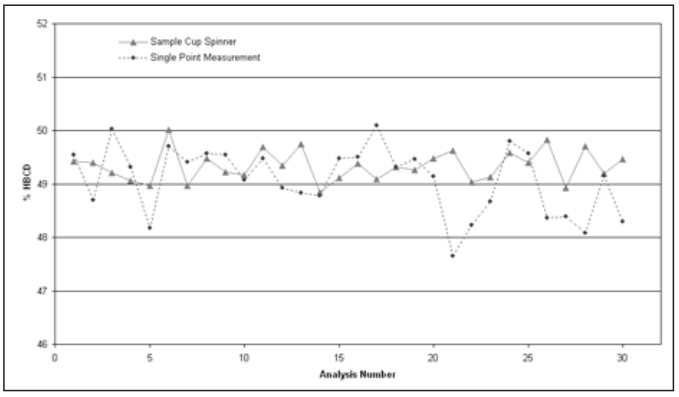

Figure 8. Variability of Sample Cup Spinner results versus single point measurement for sample 1.

Conclusions

The Antaris FT-NIR analyzer offers an excellent alternative to traditional methods for determination of additive levels in polystyrene. The main advantage of FT-NIR spectroscopy is that production efficiency is enhanced due to the quicker availability of reliable data. The use of the Sample Cup Spinner reduces the analysis time. By allowing a greater volume of sample to be analyzed, the Sample Cup Spinner provides more representative information on a heterogeneous sample and eliminates the need to analyze multiple samples from the same lot to obtain a representative result.

The data were collected using an older model instrument Antaris FT-NIR. Currently, Thermo Scientific offers an improved model, the Antaris II FT-NIR, which offers superior speed and performance over its predecessor model.

Polymerization cure rates using FT-NIR spectroscopy

Authors

Gabriela Budinova, PhD., Quintiles GesmbH, Czech Republic, Europe
Ivor Dominak, PhD., NICODOM Ltd, Czech Republic, Europe
Todd Strother, PhD.,
Thermo Fisher Scientific,
Madison, WI, USA

Keywords

Adhesive, Antaris, FT-NIR, kinetics, polymerization, spectroscopy

Figure 1. Antaris II MDS FT-NIR analyzer with integrating sphere (1a). The prepared samples were placed on top of the window over the integrating sphere, similar to what is shown in 1b, for the duration of the experiments.

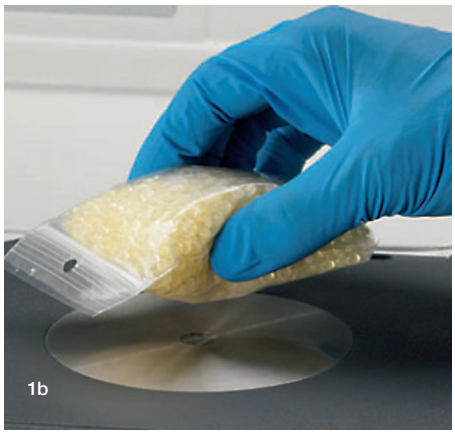

Introduction

Rate of reaction is an important parameter in chemical processes. The speed of reactions and the extent of completion often govern the viability of certain processes and determine the suitability of these reactions for commercial purposes.

One area of particular interest lies with polymerization processes. Polymerization is the general term for processes that bind single chemical units into long chains. These long chains can also cross-link to form large networks of interlocking three-dimensional structures. Plastics, epoxy-type resins and various glues and adhesives are examples of materials that are formed through polymerization processes. Fourier transform near-infrared (FT-NIR) spectroscopy can be used to study reaction rates and is used here specifically to monitor polymerization of three types of commercially available adhesives.

Often polymers require two components: a monomer with a reactive center and a curing agent. The reactive center on the monomer may be an epoxy, alkene or alkyne, acrylate, carbonyl or other functional group. The curing agent initiates or catalyzes the polymerization process through cationic or anionic addition or some other free-radical mechanism. Three polymer adhesives were the subject of this study: 1) an epoxy resin, where the epoxy functional group on the monomer is bound to amines in the curing agent; 2) a methyl acrylate adhesive, where addition to the alkene functional group is catalyzed by a free radical initiator; and 3) a cyanoacrylate adhesive, containing a similar alkene functional group, but is instead catalyzed by the presence of water vapor in air.

Near-infrared spectroscopy takes advantage of the vibrational overtones and combination bands present in nearly all complex molecules. Light from an FT-NIR analyzer impinges on the sample, causing molecular vibrations at characteristic frequencies. The light is then collected by the analyzer and is displayed as spectra. Specific substances result in unique spectra that can be used for identification or quantification. For the current study, spectra of three polymer precursors were taken at various intervals during polymerization. Peak heights at specific frequencies were measured during the experiments as a demonstration of the analyzer's ability to monitor polymer cure rates.

Experimental

Sample 1: A two-component epoxy resin (Spolchemie, Czech Republic) was obtained and mixed according to the manufacturer's recommended protocol. Samples of the activated mix were collected and prepared for analysis with a Thermo Scientific™ Antaris™ II MDS FT-NIR (Figure 1). Spectra were collected for approximately 55 hours, during which the epoxy moieties were chemically altered by nucleophilic attack from the amines in the curing agent.

Sample 2: A two-component acrylate base adhesive (UHU GmbH & Co, Bühl, Germany) was obtained from the manufacturer and mixed according to the recommended protocol. The transparent viscous acrylate copolymer contained a mixture of polymethylmethacryate and methylmethacrylate monomers and was activated by free radicals generated from dibenzoylperoxide in the powdered curing agent. Samples of this acrylate-based adhesive were prepared for FT-NIR analysis as in sample 1. Spectra were collected for approximately 20 hours, during which the alkene functionalities disappeared through an additional mechanism.

Sample 3: A rapid-setting cyanoacrylate-based adhesive (Alteco, Osaka, Japan) undergoes anionic polymerization promoted by the presence of water vapor in air. As in sample 2, the carbon-carbon double bonds of the alkenes disappear as polymerization progresses. Samples of this material were analyzed with the Antaris FT-NIR without any preparation. While the reaction time is rapid, complete polymerization requires several hours, so the samples were analyzed for approximately 20 hours.

Data acquisition: The samples above were placed on a 0.5mm thick polyethylene film covering the integrating sphere. The signal contribution of the polyethylene film was ignored in the data analysis obtained from the samples. The samples were covered with aluminum foil to allow for beam reflection. Spectra were collected between 4000 and 10000 cm^{-1}; scan resolution was set to 4 cm^{-1} and Norton-Beer apodization was used. The internal gold flag of the integrating sphere was used as the background. Simple baseline-corrected peak heights were measured at appropriate frequencies and monitored throughout the reactions.

Results and discussion

Sample 1: Figure 2a shows an overlay of spectra collected during the polymerization of the epoxy based resin in the region between 4488 – 4588 cm^{-1}. The absorption band at 4528 cm^{-1} associated with the epoxide group is shown to decrease in intensity throughout the data collection. The baseline-corrected peak height of the 4528 cm^{-1} band was plotted as a function of time (Figure 2b). The plot demonstrates that the peak height rapidly decreases in the first 1000 minutes (approximately 17 hours) essentially reaching its limit in approximately 2000 minutes (33 hours). This indicates that the reaction and curing process is complete in this time.

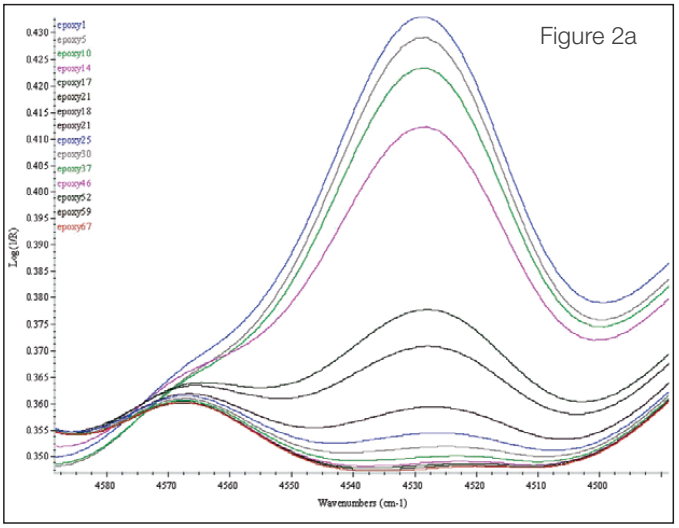

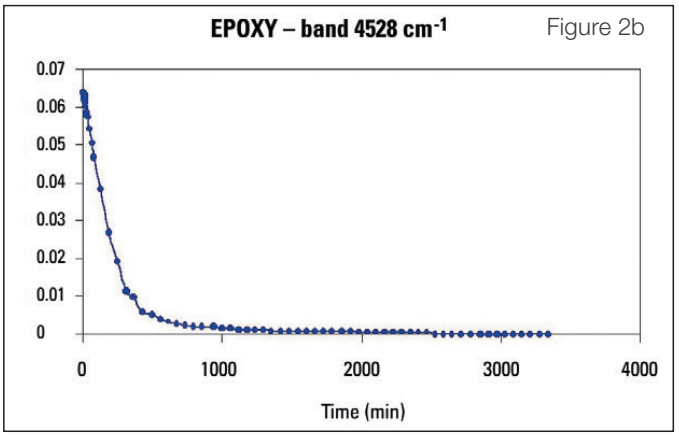

Figure 2. Overlay of spectrum showing decrease in absorption band at 4528 cm^{-1} over time (2a). Plot of the baseline-corrected peak height as a function of time (2b). The peak clearly diminishes over time as the epoxide group disappears during the polymerization process.

Sample 2: Figure 3a shows the overlaid spectra between 6103 and 6234 cm^{-1}. Here the band at 6167 cm^{-1} decreases as the polymerization progresses. This band is associated with the first overtone C-H stretch of an alkene. The baseline-corrected peak height of this band was also plotted as a function of time (Figure 3b). This plot shows a rapid decrease in peak height for the first 50 minutes, followed by a gradual decrease out to approximately 1200 minutes (20 hours). It should also be noted that the shape of the plot indicates there may be two or more chemical mechanisms accounting for the decrease in peak height.

Sample 3: Figure 4a shows the overlaid spectra of one absorption band in the range between 4450 and 4590 cm^{-1}. As expected, the peak at 4495 cm^{-1} diminishes as the polymerization progresses. Similar results were seen with bands at 4742 and 6208 cm^{-1}. The peak heights at 4495 cm^{-1} were plotted over time (Figure 4b). The plot indicates that the polymerization rapidly occurred in the first few minutes and was essentially complete by 800 minutes (approximately 13 hours). This is expected behavior for this type of rapid-setting adhesive.

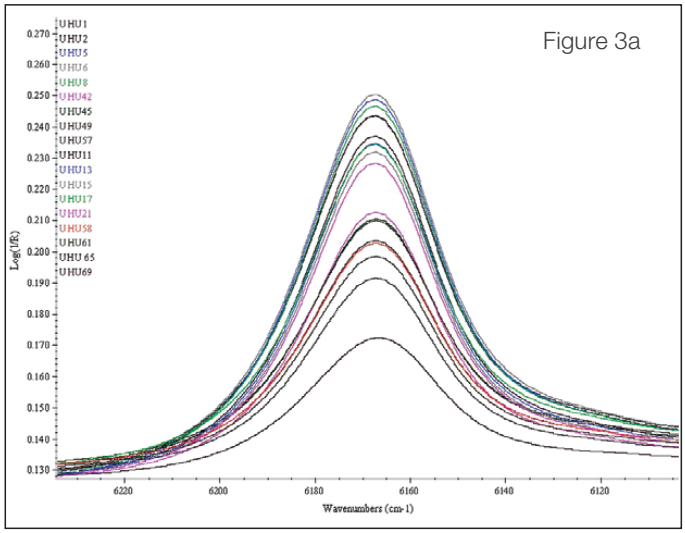

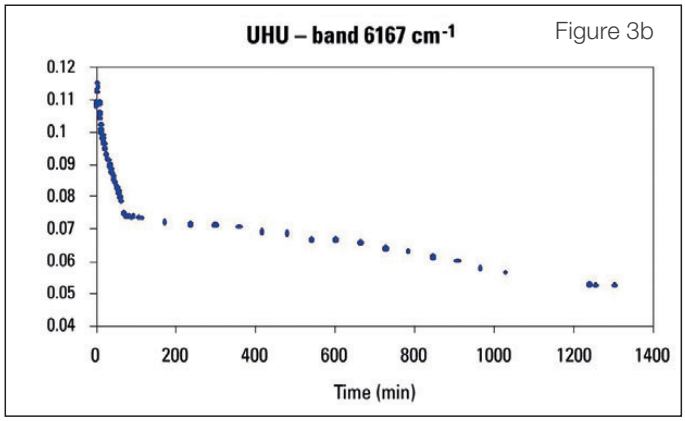

Figure 3. Overlay of spectrum in the range between 6103 and 6234 cm^{-1} for acrylate-based adhesive showing a decrease in peak height over time (3a). Plot of the baseline-corrected peak height as a function of time (3b) indicates the loss of alkene groups is initially rapid, followed by a slower gradual decrease.

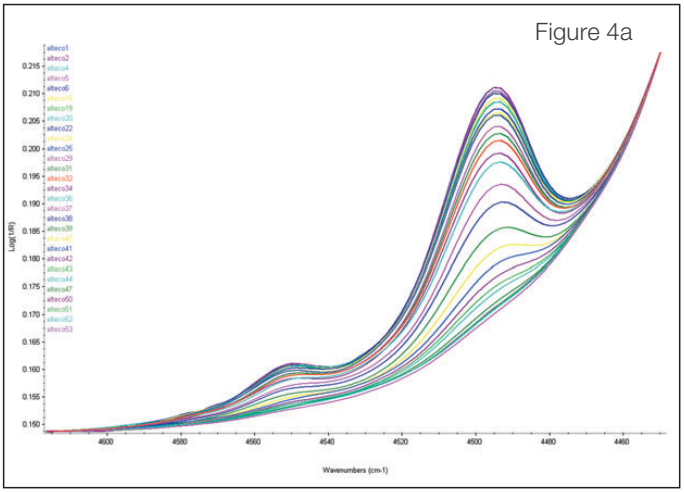

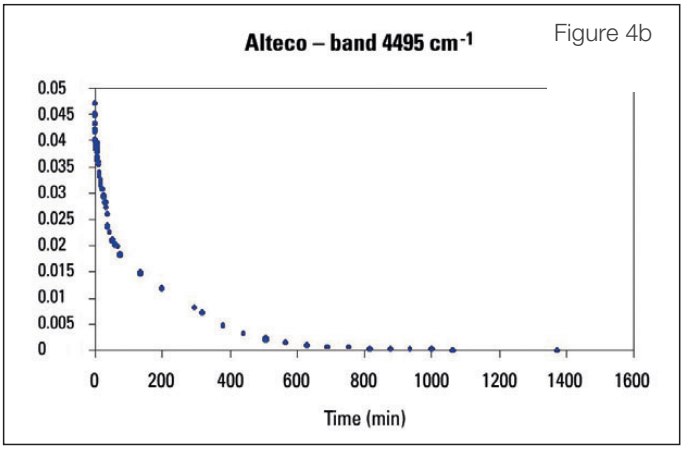

Figure 4. Overlay of spectrum in the range between 4450 and 4590 cm^{-1} for rapid polymerizing cyanoacrylate adhesive (4a). Plot of the peak at 4495 cm^{-1} as a function of time (4b) graphically demonstrates the rapid decrease in peak height associated with the rapid polymerization of this material.

Conclusion

The Antaris II FT-NIR analyzer was successfully used to monitor and track the chemical reaction rates of three polymerization reactions. An epoxy type polymer was shown to gradually cure with the loss of essentially all of the reactive groups by 2000 minutes. Polymerization of an acrylate-based adhesive was also monitored with the Antaris analyzer, with the reaction essentially complete within 1200 minutes. Finally, functional groups of a rapid-setting cyanoacrylate adhesive were shown to decrease as polymerization progressed, with the reaction essentially complete within 800 minutes. These examples clearly demonstrate the value of using the Antaris II FT-NIR analyzer to monitor reaction rates and observe reaction completion..

Density and copolymer content in polyethylene samples by FT-NIR spectroscopy

Authors

Ján Pásztor, Ladislav Tenkl, Nicolet CZ s.r.o., Prague, Czech Republic

Todd Strother, Jeff Hirsch, Thermo Fisher Scientific, Madison, WI, USA

Keywords

- Antaris
- FT-NIR Spectroscopy
- Plastic
- Polyethylene
- Polymer

Introduction

Polymer plastics have become ubiquitous worldwide and include some of the most important and useful materials available. The plastics industry is one of the largest manufacturing segments in the U.S. accounting for almost $4 billion in shipments and employing over 1 million people. Common synthetic polymers include polypropylene, polyethylene, polyvinyl chloride, polyamide and polyester. However, in addition to their advancing use and value, increasing awareness has been given to their environmental impact, both in regard to manufacture as well as post-use. Significant attention is being directed to recycling these plastics in order to minimize their environmental impact and to reduce the need for petrochemical raw materials used in their manufacture.

The most important of these polymers both in volume of material produced as well as environmental impact may be polyethylene. Polyethylene is a thermoplastic made through the polymerization of ethene (Figure 1) and is used in packaging films, toys, barrels, plumbing pipes, molded housewares, and trash and grocery bags. A variety of different polyethylene types has been developed based mostly on density of the material and branching of the intrinsic molecular chains.

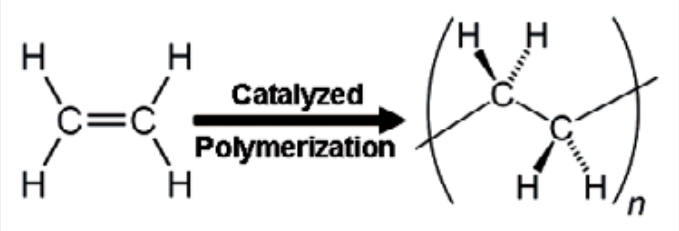

Figure 1. Catalyzed polymerization of ethene to form polyethylene.

Figure 2. Antaris MDS with sample cup spinner.

The unequivocal identification of the feedstock is of key importance in manufacturing items as well as proper recycling of these materials. Properly identifying and separating different recyclable plastics from each other so that they are processed correctly requires a great deal of effort. In addition to separating polyethylene items from other plastics, different types (densities) of polyethylene need to be separated as do items co-polymerized with other types of plastics. Unfortunately, this is often difficult to do without complex chemical analysis.

Fourier transform near infrared provides a means to identify and analyze various polyethylenes. The Thermo Scientific™ Antaris™ line of FT-NIR analyzers has proven to be useful for identifying and measuring a wide range of materials quickly and easily with no sample preparation. The Thermo Scientific™ Antaris™ II Method Development Sampling (MDS) system (Figure 2) was used to perform in-depth analyses of different densities of polyethylene as well as the amount of ethylene present in polypropylene samples.

Experimental

Two separate studies on different polyethylene materials were performed. The first focuses on classifying polyethylene samples of different densities, and development of a quantitative prediction of polyethylene densities. The second illustrates the ability of the Antaris II to quantify the amount of polyethylene in polypropylene copolymers.

Study 1

Three sets of polyethylene samples with distinct density ranges (Table 1) were analyzed using the Antaris II MDS system's integrating sphere module with a spinning sample cup. The materials were classified as either linear low density polyethylene (LLDPE, density 0.9170-0.9200 g/cm^3); medium density polyethylene (MDPE, density 0.9260-0.9400g/cm^3); or high density polyethylene (HDPE, density range >0.941g/cm^3). Each of the samples was scanned in the range between 10,000 and 4000 cm^{-1}. A discriminant analysis chemometric model was developed using TQ Analyst™ software. The first derivative spectra were analyzed between 6000 and 5700 cm^{-1} (Figure 3) where there was clear spectral difference between the three groups of materials. A Norris derivative smoothing filter was applied to the spectra before the chemometric modeling.

Sample Number	Density (g/cm^3)	Actual Class	Predicted Class
1	0.9170	LLDPE	LLDPE
2	0.9170	LLDPE	LLDPE
3	0.9173	LLDPE	LLDPE
4	0.9178	LLDPE	LLDPE
5	0.9179	LLDPE	LLDPE
6	0.9180	LLDPE	LLDPE
7	0.9180	LLDPE	LLDPE
8	0.9182	LLDPE	LLDPE
9	0.9287	LLDPE	LLDPE
10	0.9192	LLDPE	LLDPE
11	0.9200	LLDPE	LLDPE
12	0.9340	MDPE	MDPE
13	0.9340	MDPE	MDPE
14	0.9348	MDPE	MDPE
15	0.9350	MDPE	MDPE
16	0.9360	MDPE	MDPE
17	0.9360	MDPE	MDPE
18	0.9360	MDPE	MDPE
19	0.9365	MDPE	MDPE
20	0.9370	MDPE	MDPE
21	0.9376	MDPE	MDPE
22	0.9380	MDPE	MDPE
23	0.9386	MDPE	MDPE
24	0.9388	MDPE	MDPE
25	0.9395	MDPE	MDPE
26	0.9590	HDPE	HDPE
27	0.9590	HDPE	HDPE
28	0.9590	HDPE	HDPE
29	0.9595	HDPE	HDPE
30	0.9595	HDPE	HDPE
31	0.9595	HDPE	HDPE
32	0.9597	HDPE	HDPE
33	0.9598	HDPE	HDPE
34	0.9600	HDPE	HDPE

Table 1. Density and classification of polyethylene materials analyzed. All samples were correctly predicted.

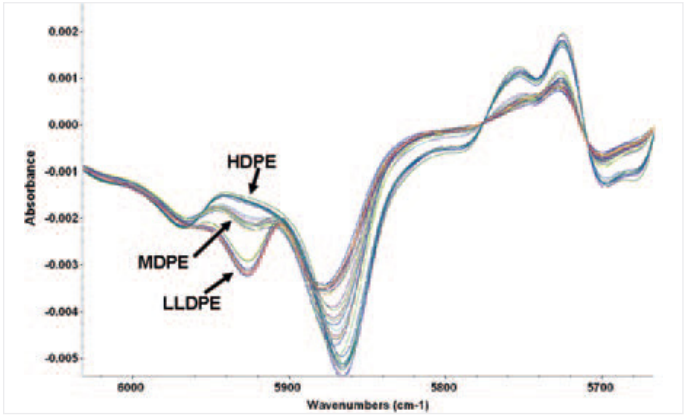

Figure 3. First derivative spectral range analyzed for discriminant analysis of the different polyethylene density classes.

The principal component scores plot (Figure 4) shows excellent separation of the different density classes. Principal components describe the spectral variation in a discriminant analysis. The first principal component describes most of the variation within the standard spectra and each subsequent principal component describes the remaining variation. Figure 4 plots the spectra against the first and second principal component. The separation between the different density classes of polyethylene indicate these materials can be successfully classified with the Thermo Scientific™ Antaris™ NIR analyzer.

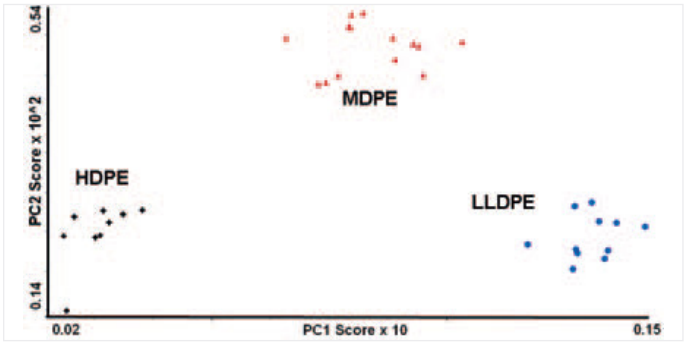

Figure 4. Principal component scores plot demonstrating clear spectral separation between the different density classes of polyethylene.

In addition to qualitatively classifying different polyethylene materials, a quantitative analysis was performed on the MDPE samples. The 11 samples of MDPE ranging in density from 0.9340 to 0.9395 g/cm3 were re-analyzed using a partial least squares (PLS) chemometric model. The unprocessed spectra were analyzed in the range from 10,000 to 6200 cm^{-1} using a 1 point baseline correction at 8840 cm^{-1}. A plot of the chemometric model's calculated values vs. actual values indicates that density can be accurately predicted (Figure 5). Selected validation spectra provide a root mean standard error of prediction (RMSEP) of 0.0005 g/cm3 with a correlation coefficient of 0.97699.

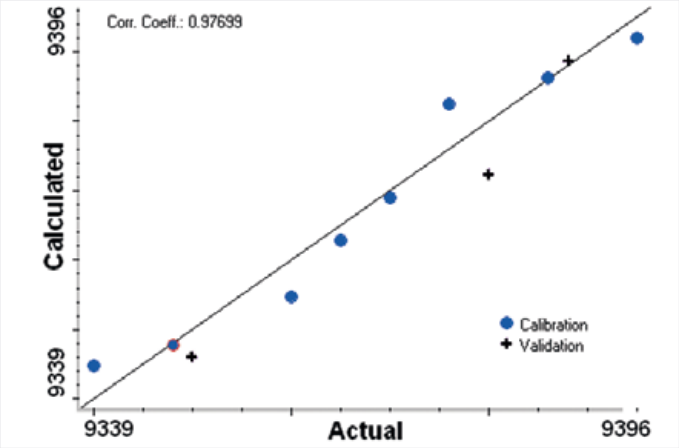

Figure 5. Regression plot showing the fit of the chemometric model for the MDPE samples. Root Mean Square Error of Prediction (RMSEP) = 0.0005.

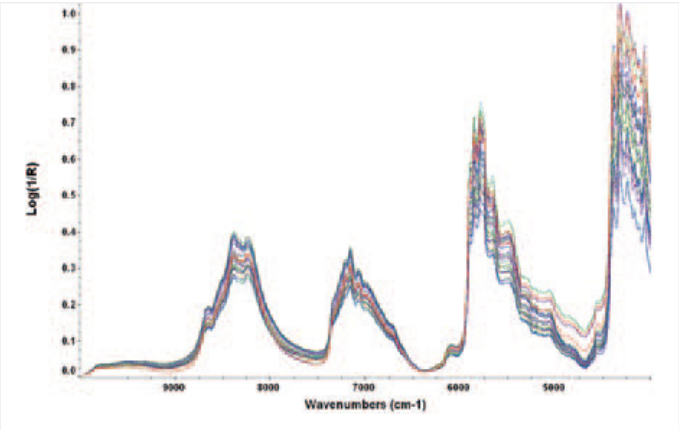

Figure 6. Spectra of ethylene-polypropylene copolymer samples. Concentration of polyethylene ranged from 2% to 16%.

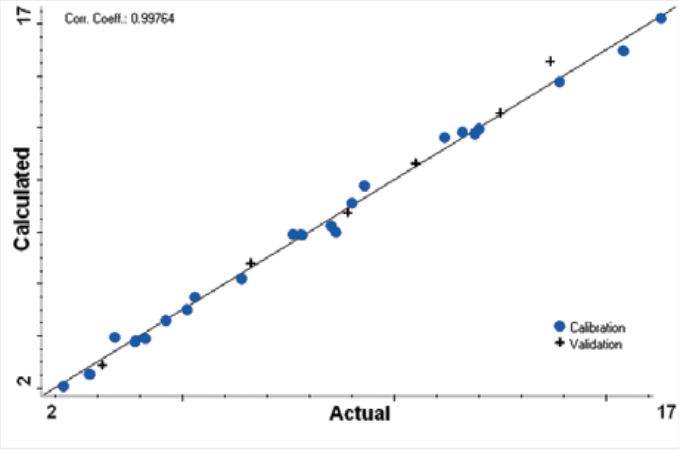

Figure 7. Regression plot of the calculated vs. actual values for the ethylenepolypropylene copolymer samples. RMSEP = 0.386.

Study 2

Polypropylene films containing ethylene as a copolymer have better clarity and lower melting points than polypropylene alone. These characteristics make such materials useful in low temperature heat-sealable applications. Melting points are linearly related to ethylene content, which makes ethylene an important measurable component. For this study, a series of 28 random and impact ethylene-polypropylene copolymer samples containing various amounts of ethylene (2% to 16%) were scanned with the Antaris II MDS system. A PLS method of analysis was selected using Thermo Scientific™ TQ Analyst™ software. The unsmoothed unprocessed spectra were analyzed between 9000 and 4500 cm^{-1} using a one point baseline correction at 9029 cm^{-1}. Figure 6 shows the spectra used in the analysis. A plot of the predicted vs. actual values of ethylene concentration in polypropylene is shown in Figure 7 and demonstrates an excellent fit. The model produces a RMSEP of less than 0.4% ethylene with a correlation coefficient of 0.99764.

Conclusion

The feasibility of both qualitative and quantitative analysis of polymeric materials using the Antaris FT-NIR analyzer has been clearly demonstrated. Specifically, polyethylene is correctly separated into different groups. Additionally, the density of MDPE is accurately predicted, and the levels of blends in an ethylene-polypropylene copolymer are accurately predicted.

ThermoFisher SCIENTIFIC

Notes

Learn more at **thermofisher.com/polymeranalysis**

thermo scientific